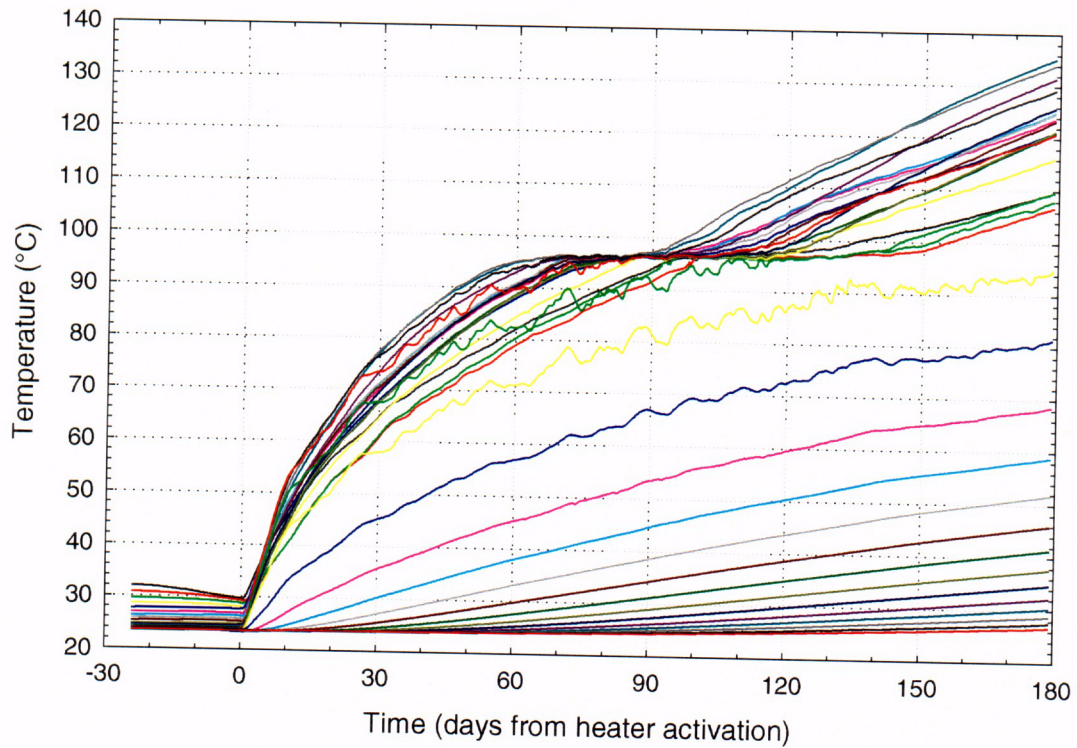


(a)



(b)

Figure 3-35. (a) Temperature every 10 days vs. distance from the borehole collar and (b) temperature of every other temperature gage vs. time for borehole 160. An animated version of (a) is in CD file *bh160.avi*.

C 29

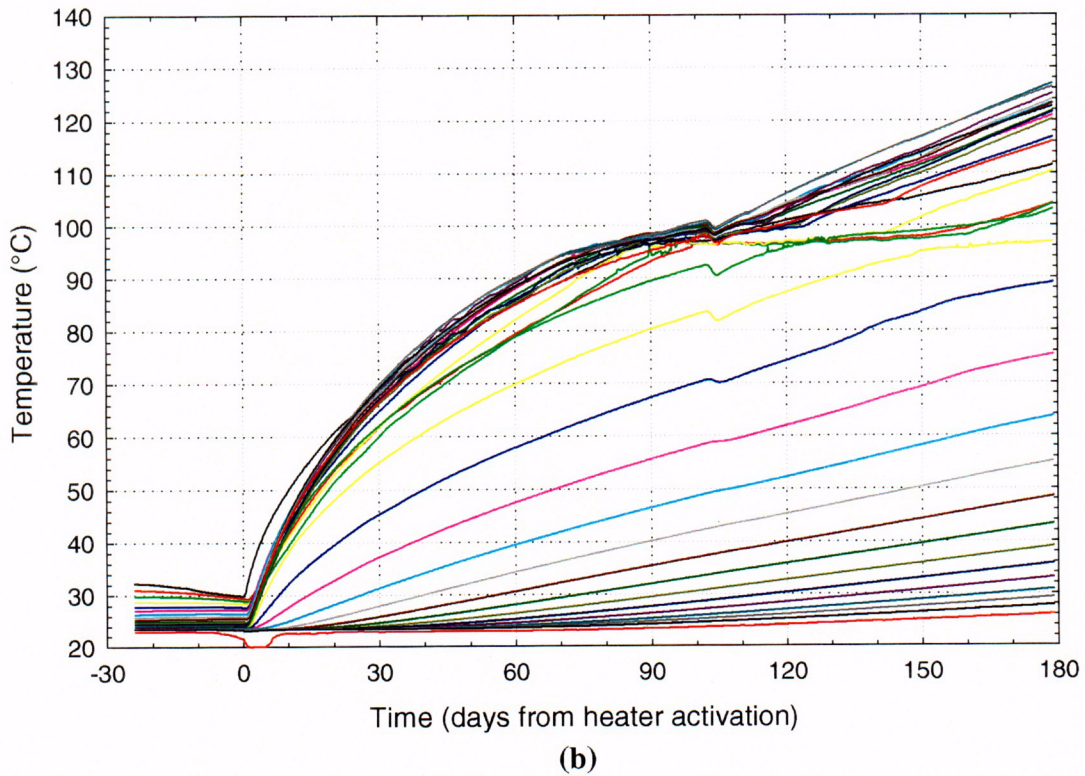
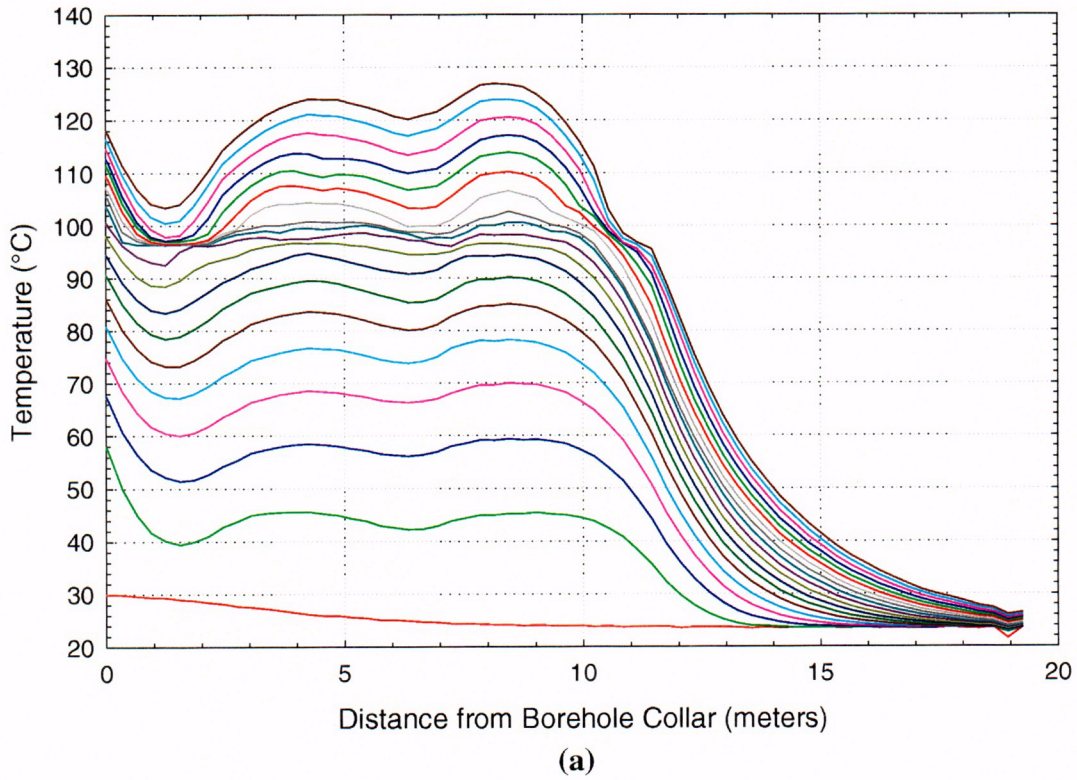


Figure 3-36. (a) Temperature every 10 days vs. distance from the borehole collar and (b) temperature of every other temperature gage vs. time for borehole 164. An animated version of (a) is in CD file *bh164.avi*.

Q 30

## Temperatures in the CIP Concrete Liner and in the Concrete Invert

The available temperature data indicate that temperatures near and in the concrete in the Heated Drift are generally lower than temperatures near and in the native rock. After three months of heating the temperatures near the borehole collars for RTD holes drilled downward into the invert were about 10°C cooler than temperatures at similar locations in RTD holes drilled upward into the crown of the drift. Figure 3-20 illustrates that the temperature on the surface of the CIP concrete liner at the back end of the drift is approximately 5 °C cooler than the temperature on the surface of the rock. Also, the air temperature at the back of the drift appears to be several degrees cooler than the air temperature near the middle of the drift. A possible explanation for these latter observations is that heat is more easily conducted at the end of the Heated Drift, which would lower temperatures at the far end of the drift as compared to temperatures in the middle of the drift. This explanation cannot account for the fact that the drop in the drift surface temperature appears to be quite abrupt and to coincide with the boundary between the lined and unlined sections of the drift (Figure 3-20).

To understand these observations, one must consider how heat is transferred from the canister heaters in the Heated Drift to the rock. The heating elements in the heaters warm the outer surfaces of the canisters up to somewhere between 130 and 140 °C (Figure 3-9). From there, the heat is transferred through the air to the drift surface by radiation, convection and conduction. Radiation is probably the most important mechanism of heat transfer to the drift surface while conduction is likely insignificant since air is a very poor thermal conductor. Once heat has penetrated the surface of the drift, heat transfer is dominantly by conduction. The important material properties that determine the temperatures in the drift are the thermal conductivity, heat capacity and thermal absorptivity of the materials involved. The thermal conductivity of concrete with limestone aggregate is believed to be somewhat higher than that of tuff (3.2 vs. 2.0 W/m-K), their heat capacities are likely very similar and their absorptivities are unknown.

Consider two one-dimensional temperature profiles extending radially away from the surface of the canister heaters out into the rock. One profile penetrates the CIP concrete liner while the other does not. Figure 3-9 indicates that the surface temperatures of all the canister heaters are nearly identical, so the two profiles start out at the same temperature. Assume for a moment that the material properties are such that heat transfer into the concrete occurs at a faster rate than into the rock. This would result in cooler air temperatures and warmer rock temperature along the temperature profile with the concrete liner. Conversely, if heat transfer into concrete were more difficult than into rock, the air temperature would be warmer and the rock temperature cooler along the profile that includes the concrete liner than along the profile that does not include the liner. Neither of these is the observed pattern. Air and rock temperatures are both cooler along radial profiles through the concrete liner as compared to profiles which do not involve the liner. This implies the existence of an energy sink along the profile that penetrates the liner, which does not exist along the profile that does not involve the liner.

A possible explanation is that there is some endothermic process under way in the concrete that is lowering the temperature all along profiles which penetrate it. This may occur as the result of water loss from the concrete. Mechanically bound liquid water may be evaporating or boiling in the concrete, thereby holding down its temperature, or chemically bound water may be being released, with the same result. This possibility is supported by surface strain gage data from the concrete liner, which indicate that the concrete is experiencing dehydration shrinkage, particularly

at temperatures below 96°C. These data are discussed in more detail in Section 4.4. If this explanation is correct, the observed differences between the thermal behavior of the concrete-lined and unlined sections of the drift should decrease with time as the concrete dries out.

### Air Movement in the Rock Surrounding the Heated Drift

There are several lines of evidence suggesting that substantial amounts of air are moving through the rocks surrounding the Heated Drift. They all involve correlation of some physical parameter with barometric pressure as measured by the pressure gages located in the Heated Drift. When barometric pressure rises, air is forced into the Heated Drift and the surrounding rocks and when the pressure drops, the air is extracted from the same locations. If a gage is located in a position where there is a substantial spatial gradient of the parameter being measured, air movement past the gage will cause substantial changes in the measurements. When air flow is in the direction of increasing value of the parameter, the measurements will decrease. Conversely, when the air is flowing in the direction of decreasing value of the parameter, the measurement will increase.

### Humidity

There are two air humidity sensors deployed in the Heated Drift. They are both located near the right rib of the drift approximately 70 cm from the bulkhead. The data from these sensors are plotted in Figure 3-37, along with the air pressure measured in the Heated Drift. The data indicate that the humidity in the drift is inversely correlated with the air pressure (Figure 3-38). When barometric pressure increases, relatively dry, outside air enters the Heated Drift through gaps in the bulkhead, lowering the relative humidity. Conversely, when the barometric pressure drops, relatively moist air flows into the Heated Drift from the surrounding rocks and then out of the Heated Drift through the bulkhead, raising the relative humidity in the Heated Drift. During this process there must be exchange of air between the Heated Drift and the surrounding rock for there to be any change in the measured relative humidity. If dry air simply entered and exited the Heated Drift without flowing into the rock, the humidity would reach a steady state and then remain relatively constant. The only plausible source for the water which causes the increase in relative humidity is the water being evaporated from the pores of the rock surrounding the Heated Drift.

### Temperatures in MPBX boreholes

The temperature data from the thermocouples mounted on the MPBXs are discussed in detail in Section 4 since their primary purpose is to make thermal expansion corrections to the MPBX displacement data. They exhibit behavior that indicates air flow in the MPBX holes, however, which will be discussed here. Figure 3-39 is a plot of the temperatures measured by a thermocouple located 4.1 meters from the collar in MPBX borehole 147. This hole is located about 13 meters down the drift from the bulkhead. Because it is oriented perpendicular to the axis of the drift, the temperature gradient in the hole is substantial, on the order of 10 °C/m. The air pressure measured in the Heated Drift is also plotted in Figure 3-39. The data indicate that the temperature is well correlated with the pressure. When the pressure increases, air flows along the borehole, away from the drift, carrying relatively warm air from closer to the drift to more distal regions. Conversely, when the pressure drops, air is sucked out of the hole, causing relatively cool air from regions more distant from the drift to flow past the gage. The temperature oscillations exhibited by the thermocouple are on the order of about 15°C, indicating that substantial amounts of air are flowing in the hole with considerable velocity.

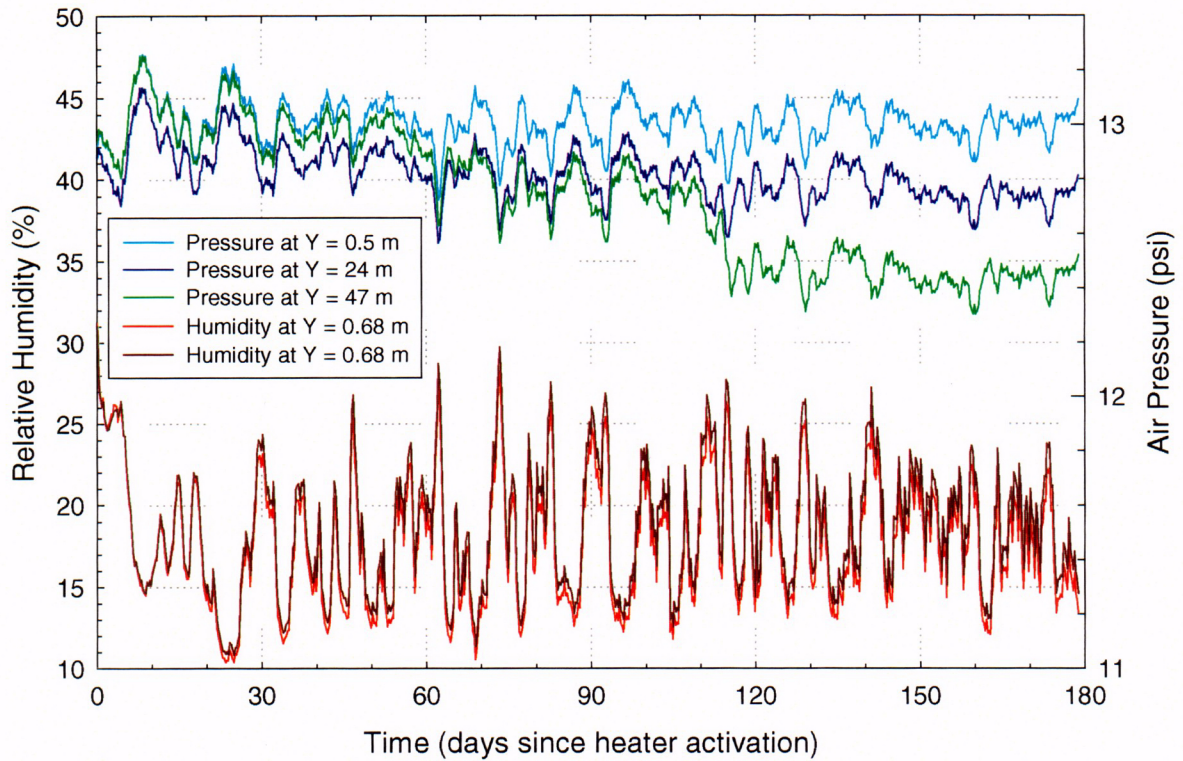


Figure 3-37. Air pressure and relative humidity in the Heated Drift as a function of time. The substantial difference in pressure measured by the three pressure sensors is unexplained at this time but is likely an instrumentation issue.

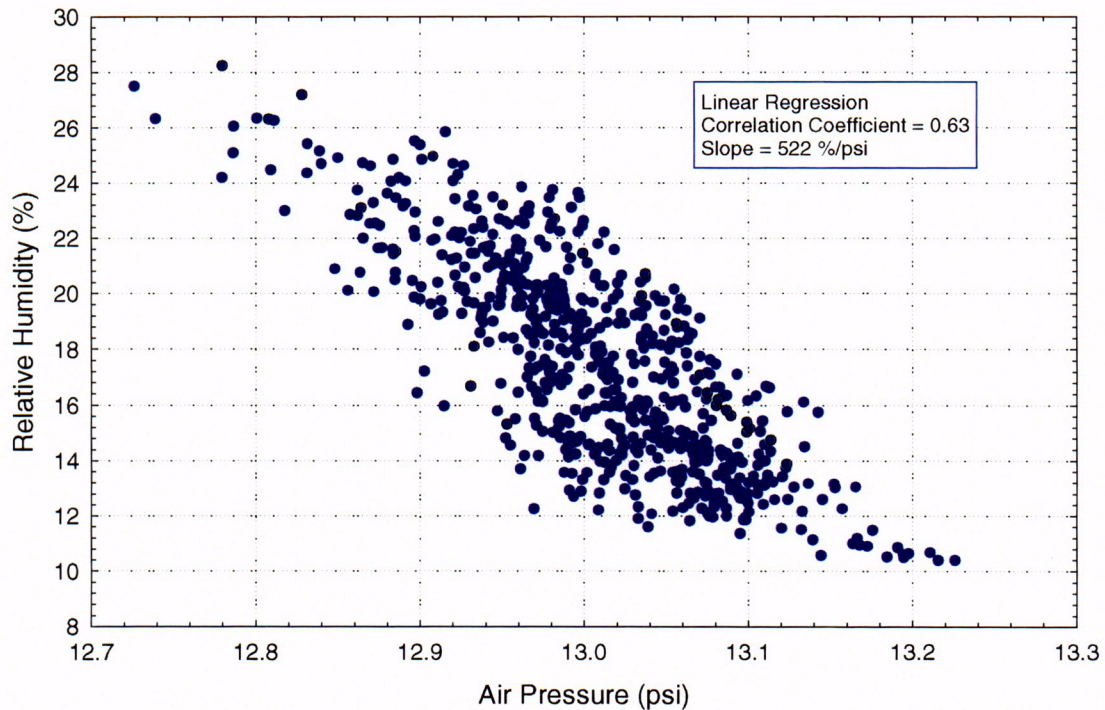


Figure 3-38. Relative humidity versus air pressure during the first 179 days of heating.

C 31

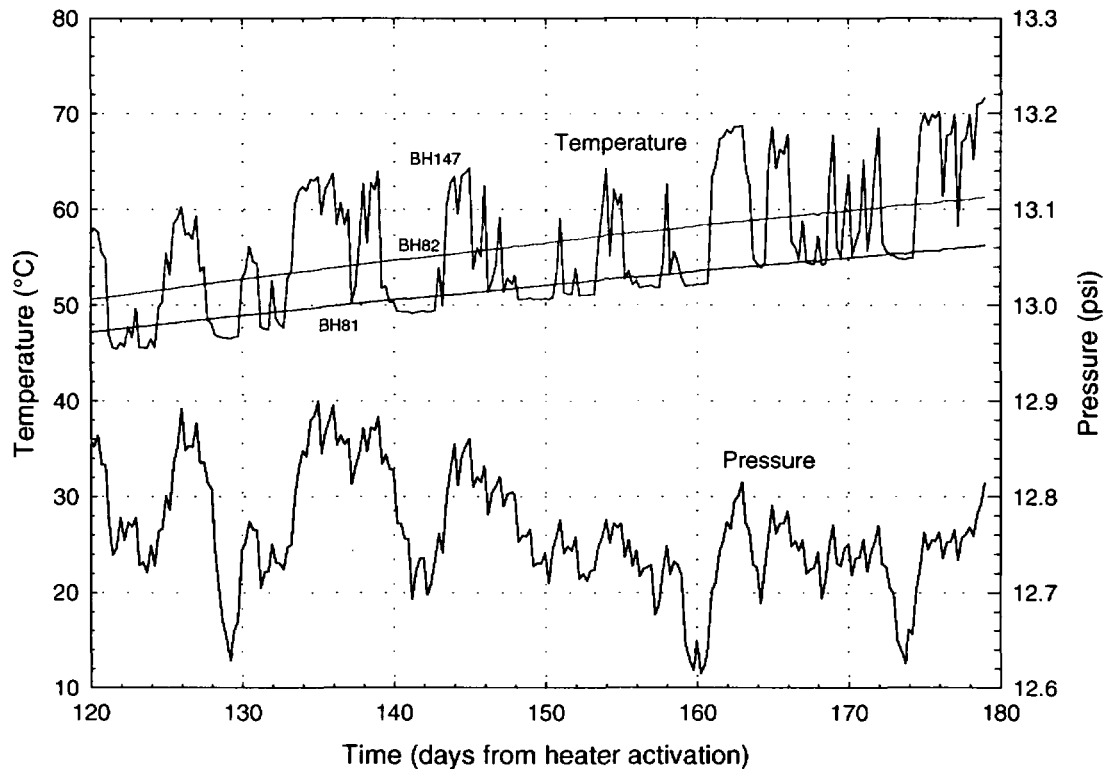


Figure 3-39. Drift air pressure and temperatures measured at thermocouple 4.1 meters from collar of MPBX borehole 147.

This much air flow cannot result merely from the compressibility of air within the volume of the borehole but must reflect air flowing into and out of the rock as well, presumably through fractures which intersect the borehole. These temperature oscillations are in evidence in all the open MPBX holes which intersect the Heated Drift. They are not observed in boreholes 80 and 81, however, which are the long horizontal holes oriented parallel to the axis of the drift. This is likely because these holes were drilled, grouted and redrilled prior to installation of the MBPX anchors. This would have plugged all the fractures that intersected the hole, thereby preventing communication between the boreholes and the surrounding rock.

#### Temperatures in RTD boreholes

There is a similar observation in some of the RTD boreholes. The yellow curve in Figure 3-35b illustrates the temperature recorded by the RTD temperature gage located in borehole 160 right adjacent to the end of the outer wing heater. Note the temperature oscillations exhibited by this gage. A few other nearby gages exhibit similar behavior. These gages are located in a region where the temperature gradient in the borehole is on the order of about 15°C/m. In Figure 3-40, the rate of change of temperature of this gage is compared to the air pressure in the Heated Drift, as a function of time. As with the MPBX data, these data indicate that when the air pressure increases, the temperatures warm and vice versa. Interpretation of this observation is complicated by the fact that this borehole is presumably sealed with grout, which should prevent air flow in the hole. Possible explanations are that the grout is either cracked or has not filled the hole, thereby allowing some air flow or that the air is flowing through a nearby fracture and not through the hole at all. These types of temperature oscillations are not observed in most of the RTD

boreholes, even though most of them are located in regions with steep temperature gradients, so the phenomenon is not widespread with respect to these holes.

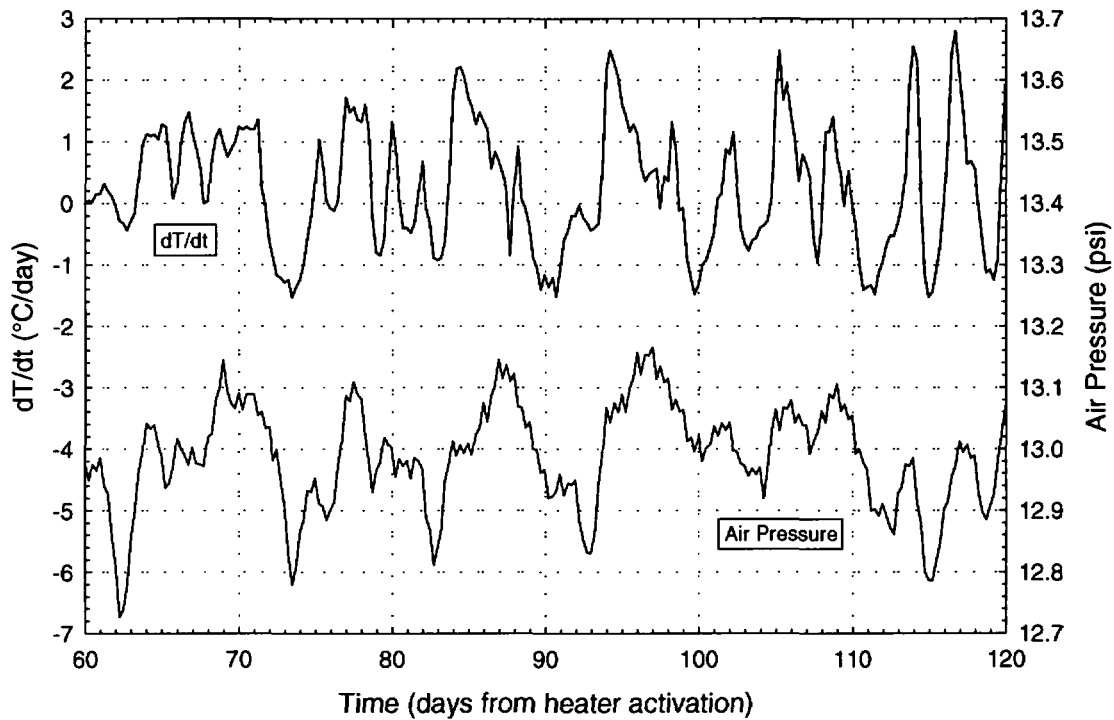


Figure 3-40. Air pressure in the Heated Drift and the rate of change of temperature measured by a gage located 11.4 meters from the drift wall in borehole 160.

Page intentionally blank

## 4. Mechanical Measurements

This section describes measurements of rock displacement, strain, and rock mass modulus. Figures summarizing displacement and strain time-histories for selected gages are presented. The mechanical data presented here were taken through May 31, 1998. Data acquired from the Plate Loading Test and used to obtain estimates of rock mass modulus are presented and discussed. A brief description of instruments and equipment is given in Appendix B. As-built gage locations are given in Appendix C. Failed and suspect gages are identified in Section 5 and Appendix D. Specific details regarding serial numbers, calibration records, etc. can be found in the Scientific Notebook covering this work.

Displacements are measured within the rock mass surrounding the Heated Drift and between the Heated Drift and the Observation Drift. These measurements are used to evaluate numerical models related to T-H-M coupling as well as to provide data for determination of rock mass thermal expansion. Strains are being measured on the inner surface of the cast-in-place liner installed in the west end of the Heated Drift. Displacements and strains in the Heated Drift reported in this document follow the convention of extension being positive. For the Plate Loading Test, because it is a compressive test, pressures and displacements follow the convention of compression being positive for easier manipulation of the data.

An additional activity evaluating the mechanical behavior observed in the Drift Scale Test is a suite of laboratory tests (in progress) designed to assist in the characterization of materials used in the cast-in-place (CIP) concrete liner in the Heated Drift. Specimens of concrete were cast into specimen molds during emplacement of the concrete liner. Thermal expansion measurements and constant load (creep) tests have been initiated on these specimens at temperatures up to 200°C. The interim results of these tests are given in Appendix E of this report.

### 4.1 Displacement Measurements—Borehole MPBXs in the Heated Drift

Multiple point borehole extensometers (MPBXs) were installed in 17 boreholes both within and outside the Heated Drift to monitor rock mass movement during the DST (see Figures 2-1, 2-2, and 2-3). Two of the MPBXs (designated ESF-HD-81-MPBX1 and ESF-HD-82-MPBX2; 81 and 82 refer to the borehole numbers) were installed in two long horizontal boreholes drilled parallel to the Heated Drift from the connecting drift. Twelve MPBXs (MPBX3 through MPBX14; their designations include corresponding borehole numbers—see Table C-3) were installed in three four-borehole arrays drilled into the surrounding rock mass from within the Heated Drift itself. This section presents the results of these 14 MPBXs. The other three borehole MPBXs were drilled for sequential mine-by monitoring, and will be discussed in Section 4.3. Two cross-drift extensometers (CDEXs) were installed in the section of the Heated Drift with a cast-in-place concrete liner to measure cross-drift convergence; the results of these CDEXs are discussed in Section 4.2.

Because of an ongoing quality assurance (QA) Deficiency Report YM-97-C-004 regarding procurement and issues with the manufacturer (GEOKON) of the C-ring anchors, vibrating wire transducers, and linear variable displacement transducers, the displacement measurements from all the MPBXs and CDEXs are currently not qualified per YMP QA procedures. It is anticipated that the data will be qualified upon resolution of the QA issues.

Two horizontal boreholes drilled parallel to the Heated Drift from the Connecting Drift (borehole numbers 81 and 82) were instrumented with GEOKON C-ring six-anchor MPBXs. Each of the C-ring anchors was connected to a Delrin MPBX head (located at the borehole collar) via Invar connecting rods. A vibrating wire displacement transducer is attached to each connecting rod to measure the relative displacement between the anchors and MPBX head which is fixed and sealed into the borehole collar. There is a total of twelve vibrating wire gages installed in these two boreholes for the DST.

Twelve boreholes in three four-borehole arrays (numbers 147-150, 154-157, 178-181) were drilled into the surrounding rock mass from within the Heated Drift itself. The array setup is shown in Figure 4-1. The array containing MPBXs 3, 4, 5, and 6 (boreholes 147-150) is located in the Heated Drift at  $y=13.7$  m; the array with MPBXs 7, 8, 9, and 10 (boreholes 154-157) is located at  $y=21.0$  m; and the array with MPBXs 11, 12, 13, and 14 (boreholes 178-181) is located at  $y=41.1$  m, in the concrete liner test section of the Heated Drift. Each of these boreholes was instrumented with an MPBX that included four GEOKON C-ring anchors with Invar connecting rods. The displacements are measured relative to the MPBX heads, which are made of type 316 stainless steel and are fixed and sealed into the borehole collar. Displacements were measured using high temperature linear variable displacement transformers (LVDTs) fixed in each stainless steel head. The LVDTs were manufactured by RDP Electrosense, Inc. A total of forty-eight high temperature LVDTs is used in the twelve MPBXs within the Heated Drift. For the three MPBXs in each array collared in the crown of the drift, the four anchors for each were located nominally at 1, 2, 4, and 15 m from the collar. For the fourth MPBX in each array, which was collared at the top of the invert, the anchors were installed so as to put them in the same relative position in the surrounding rock mass as the other MPBXs (i.e., approximately 2.2, 3.2, 5.2, and 16.2 m from the collar). As-built locations for each anchor are given in Appendix C.

For all borehole MPBXs, temperature measurements are made using Type-K (chromel-alumel) mineral-insulated/metallic-sheathed ungrounded thermocouples along the lengths of each MPBX. Ungrounded in this case refers to the thermocouple junction itself which is electrically insulated from the stainless steel sheath. These temperature measurements allow for computation of displacement compensation for rod thermal expansion effects. The locations of the anchors and individual thermocouple junctions were determined from the survey and borehole collar coordinates, from the field notes for installation (e.g., installed depth to various anchors and points on the MPBXs), and from manufacturers' and SNL specifications for the MPBXs. The extension wires for the displacement gages were either mineral-insulated/metallic-sheathed for the high temperature LVDT within the Heated Drift, or standard instrumentation hookup wire for the vibrating wire displacement transducers for the gages located in the Observation Drift and the Connecting Drift.

All of the MPBX boreholes were open (not grouted), so that convective air flow within the boreholes is possible. To minimize the influence of open boreholes on rock temperature distributions, the boreholes were sealed using aluminum tubing coated with Teflon. As a result, temperature measurements in the MPBX boreholes do not reflect rock temperature and are used only to correct displacement measurements for rod thermal expansion.

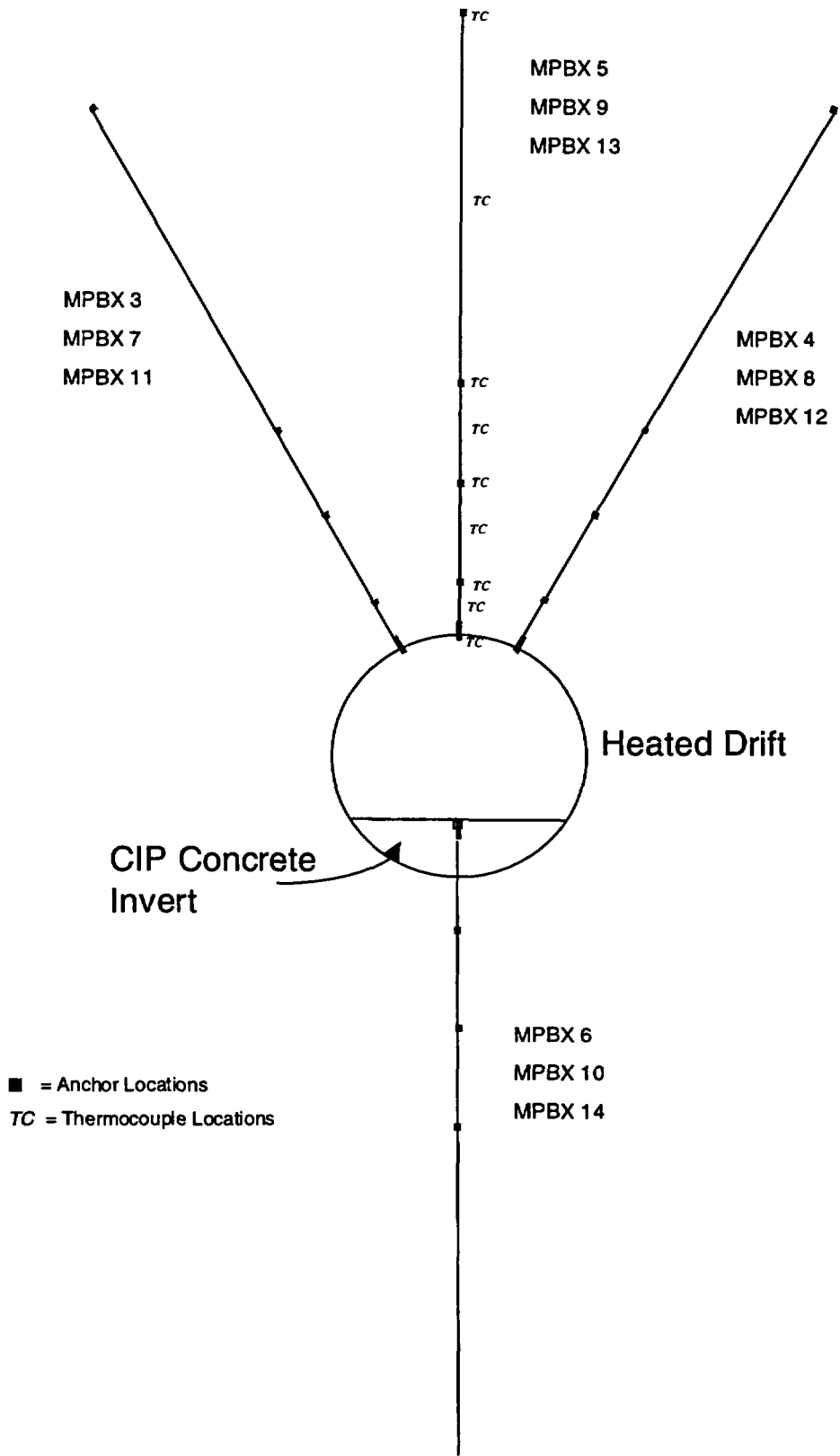


Figure 4-1. MPBX layout in the Heated Drift.

Gage and anchor locations (as-builts) for displacement measurements made for the DST are presented in detail in Appendix C of this report and additional information can be found in TDIF #306548 (DTN: SNF38040197001.001). Specifications for the gages are given in Appendix B of this report.

The thermal expansion of the thin Invar rods that are used to connect MPBX anchors to the displacement sensors located in the MPBX head (collar) and of the cross-drift extensometers (CDEX) must be determined. The rod thermal expansion must be added to the measured displacements to obtain the actual rock mass displacements. Because the rods expand due to heating, the displacements measured by the gages appear to be smaller. The actual rock mass displacements are therefore the measured displacements plus the rod expansion. The rod thermal expansion is calculated from temperatures measured on the rods, measured rod lengths, and known (SNL laboratory determined, DTN: SNL22100196001.003) Invar thermal expansion coefficients. The calculated rod thermal expansion is:

$$\delta = \alpha \Delta T \ell, \quad (4-1)$$

where:

- $\delta$  = MPBX connecting rod thermal expansion (m)
- $\alpha$  = Thermal expansion coefficient for Invar ( $10^{-6}/^{\circ}\text{C}$ )
- $\Delta T$  = Change in temperature above ambient (assumed to be  $25^{\circ}\text{C}$ )
- $\ell$  = Invar rod segment length (m)

The cumulative thermal expansion for each successive anchor for the MPBXs is the sum of the previous anchors' thermal expansions. This cumulative calculation is used because a temperature gradient is expected along the length of the MPBXs. For this calculation, the "average" temperature change over each rod segment length is used. The Invar thermal expansion coefficient has been measured in the laboratory by SNL and been found to be somewhat temperature dependent (DTN:SNL22100196001.003). Table 4-1 presents measured Invar thermal expansion coefficients over a range of temperatures that are to be used in the MPBX and CDEX rod thermal expansion correction calculation.

Table 4-1. Invar Thermal Expansion Coefficients

Temperature Range ( $^{\circ}\text{C}$ )	Thermal Expansion Coefficient ( $10^{-6}/^{\circ}\text{C}$ )
25-50	1.62
50-75	1.89
75-100	2.17
100-125	2.71
125-150	3.44
150-175	4.51
175-200	5.62
200-225	7.17

From: DTN: SNL22100196001.003, TDIF 306356

A fourth-order polynomial fit was performed to the alpha values corresponding to the midpoint temperatures (e.g., 37.5°, 62.5°, 87.5°, etc.) for each of the temperature ranges in Table 4-1 from ambient to 200°C and the  $\alpha$  values listed in the table. The resulting equation is used in conjunction with measured temperatures and Equation 4-1 to determine the thermal expansion of each of the Invar connecting rods. There are typically at least two thermocouples located within each rod segment length. The locations of the anchors and thermocouples are identified in the DST SNL "As-Built" Gage Location Table in Appendix C (DTN: SNF38040197001.001). These locations are used in the rod expansion calculation for the rod segment length and temperature change terms in Equation 4-1 above.

The MPBX data collected for the DST are presented in Figures 4-2 through 4-15. For each of these MPBXs, anchor 1 is the closest to the collar. A positive displacement indicates relative extension between anchor and collar. Figures 4-2 and 4-3 are for MPBXs installed in boreholes parallel to the Heated Drift axis (ESF-HD-MPBX1 and ESF-HD-MPBX2). These two MPBXs measure the axial deformation of the rock mass on either side of the Heated Drift using six-vibrating wire transducers mounted in heads located at the borehole collars in the Connecting Drift. The gages measure the relative displacement between the borehole collar and six anchors spaced along the borehole length. The displacements are transferred from each anchor to a respective gage via Invar rods. These gages are therefore located in a region of the Thermal Testing facility which will continue to be at ambient or near ambient temperatures during the duration of the DST. Each of these two MPBXs use six C-ring anchors spaced along the length of the boreholes to depths corresponding to coordinate locations Y=33.9 m and 34.5 m respectively. There are also twelve MPBXs (ESF-HD-MPBX3 through ESF-HD-MPBX14) which are installed in boreholes drilled from within the Heated Drift radially along three cross-sections. The locations of these MPBXs are shown in Figure 4-1. MPBX3 through MPBX14 each use, as gages, four high temperature LVDTs located in the MPBX head connected to four C-ring anchors using Invar connecting rods. An examination of the data available through May 31, 1998 suggest that several of the installed displacement gages are providing suspect data. A complete list of failed and suspect gages for the DST are given in Section 5 and Appendix D of this report.

The displacement data presented for the DST MPBXs in Figures 4-2 through 4-15 are corrected for connecting rod thermal expansion as described above. The temperatures measured along the lengths of each MPBX on day 179 (May 31, 1998) are presented in Figures 4-16 through 4-29. Because some of the thermocouples have failed or are suspect (see discussion in Section 5 and Appendix D), some of the temperature plots include fewer than the original number of installed thermocouples, and the curves are therefore less smooth than those with a full complement of operating temperature sensors. The temperature profiles exhibited in MPBXs ESF-HD-MPBX1 and ESF-HD-MPBX2 shown in Figures 4-16 and 4-17 show nearly ambient or slightly increasing temperatures from the borehole collar to a depth of about 8 m and then a sharp increase to about 66–68°C at a depth of about 16 m from the collar. The 16-m depth is roughly equivalent to about 5 m beyond the thermal bulkhead. These temperature increases are due to the wing heaters which are about 3.8 m below these boreholes. The temperature measurements for ESF-HD-MPBX3 through ESF-HD-MPBX14 presented in Figures 4-18 through 4-29 were used to calculate displacement corrections for Invar rod thermal expansion. (Note that the collar thermocouples for MPBX8 and MPBX11 failed; the collar temperatures in Figures 4-23 and 4-26 are taken from MPBX-7 and MPBX12, respectively.)

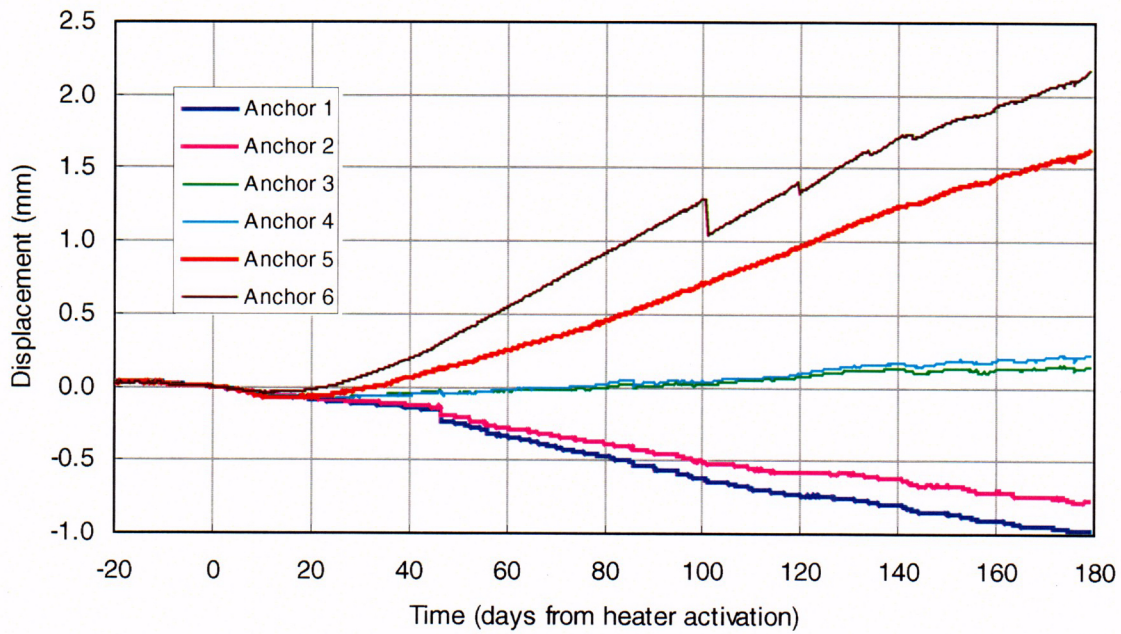


Figure 4-2. Measured displacements from ESF-HD-81-MPBX1 (corrected for thermal expansion).

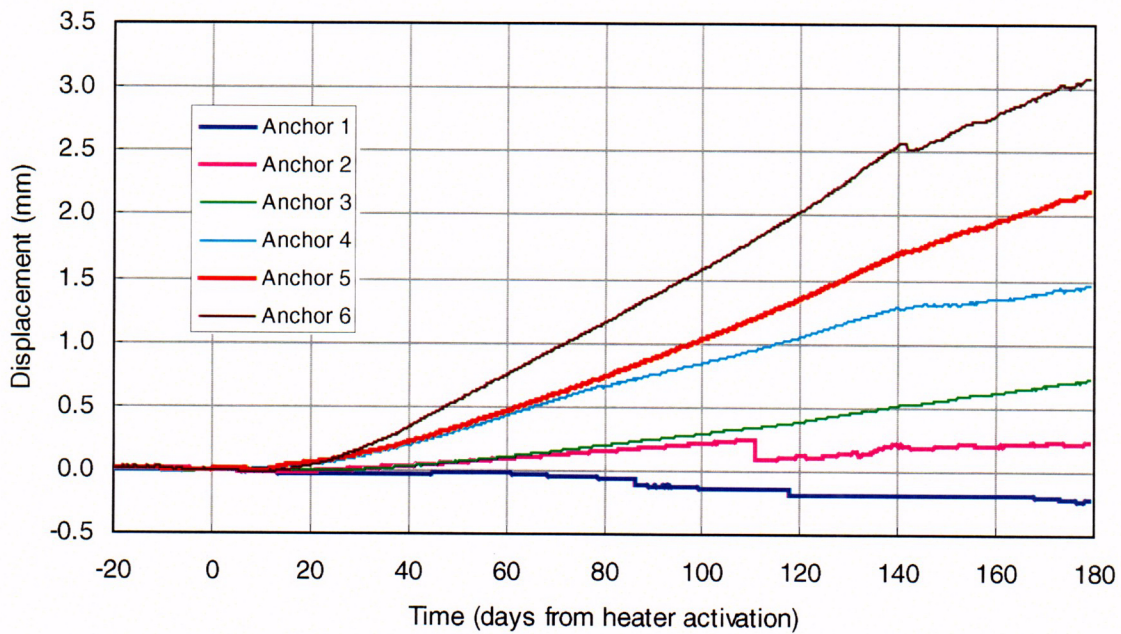


Figure 4-3. Measured displacements from ESF-HD-82-MPBX2 (corrected for thermal expansion).

C 32

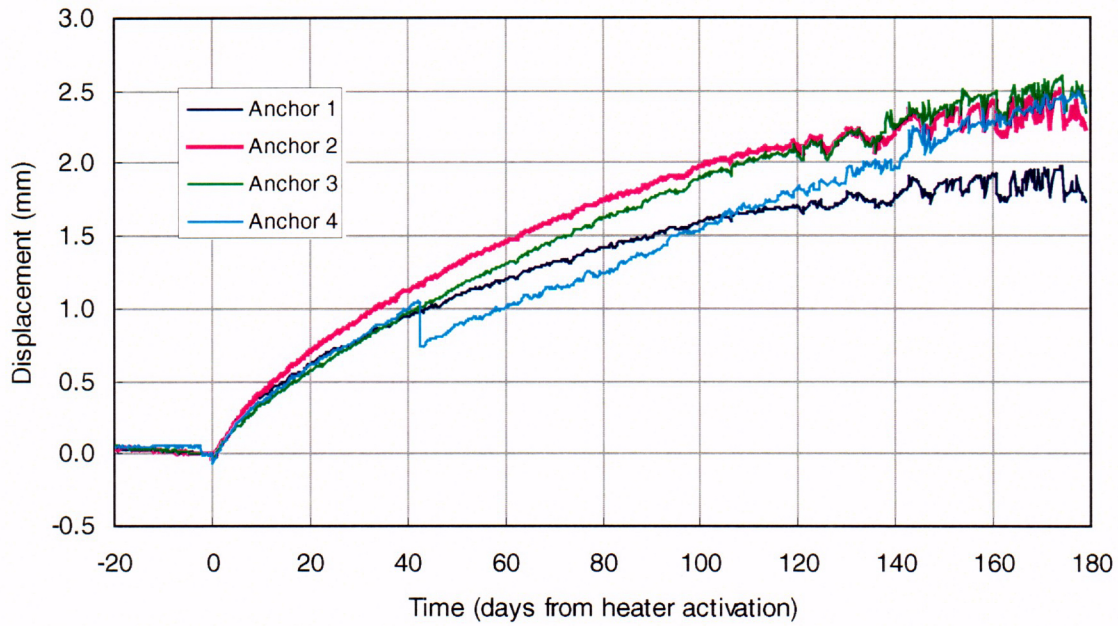


Figure 4-4. Measured displacements from ESF-HD-147-MPBX3 (corrected for thermal expansion).

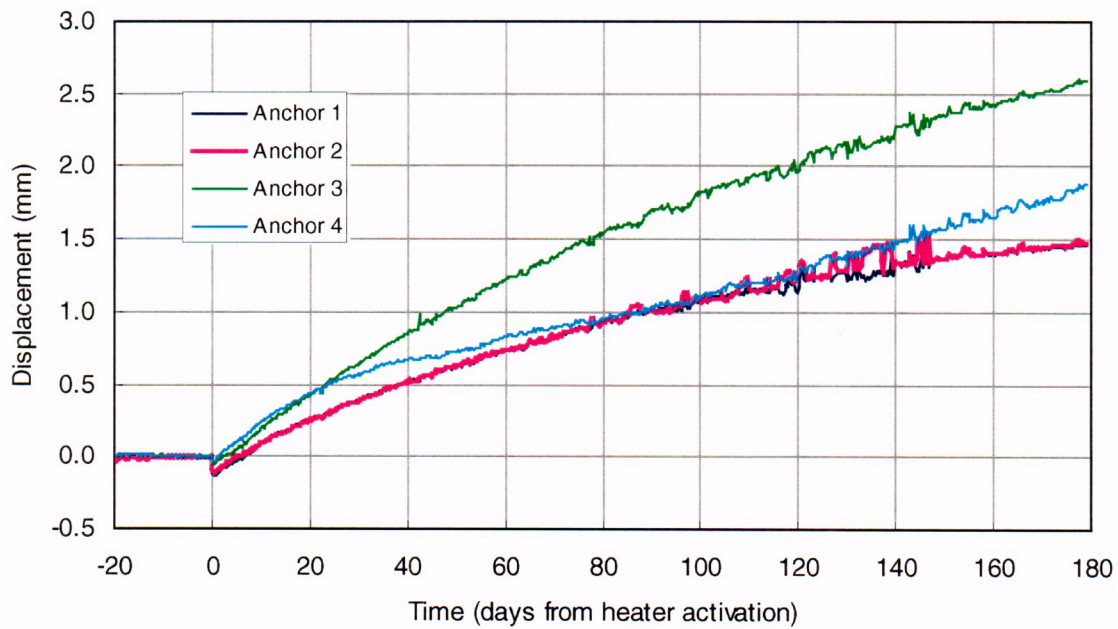


Figure 4-5. Measured displacements from ESF-HD-148-MPBX4 (corrected for thermal expansion).

C33

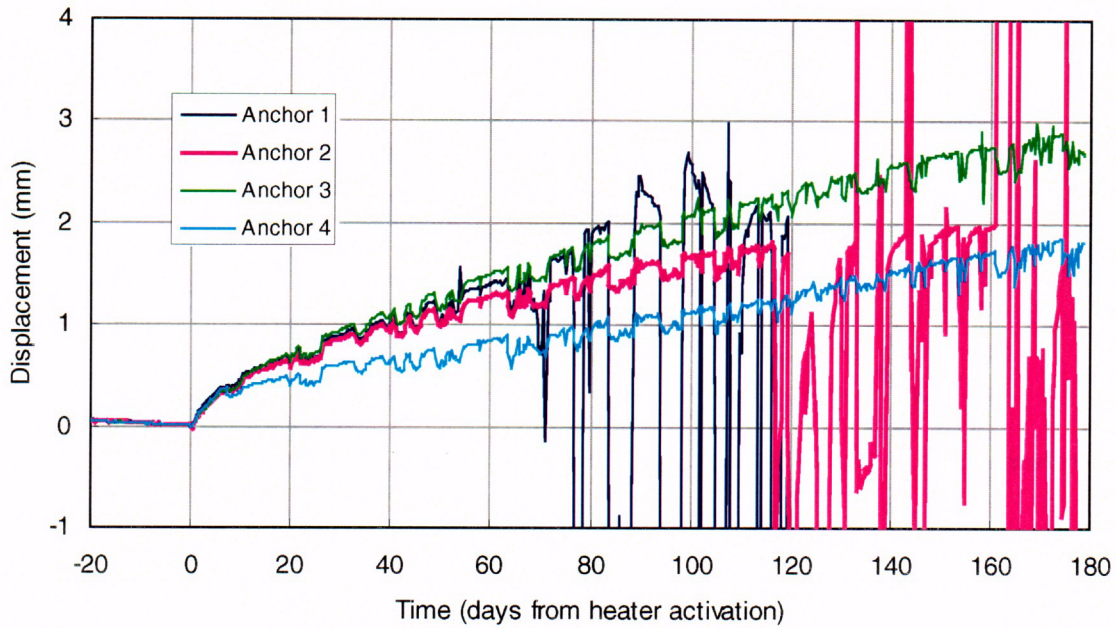


Figure 4-6. Measured displacements from ESF-HD-149-MPBX5 (corrected for thermal expansion).

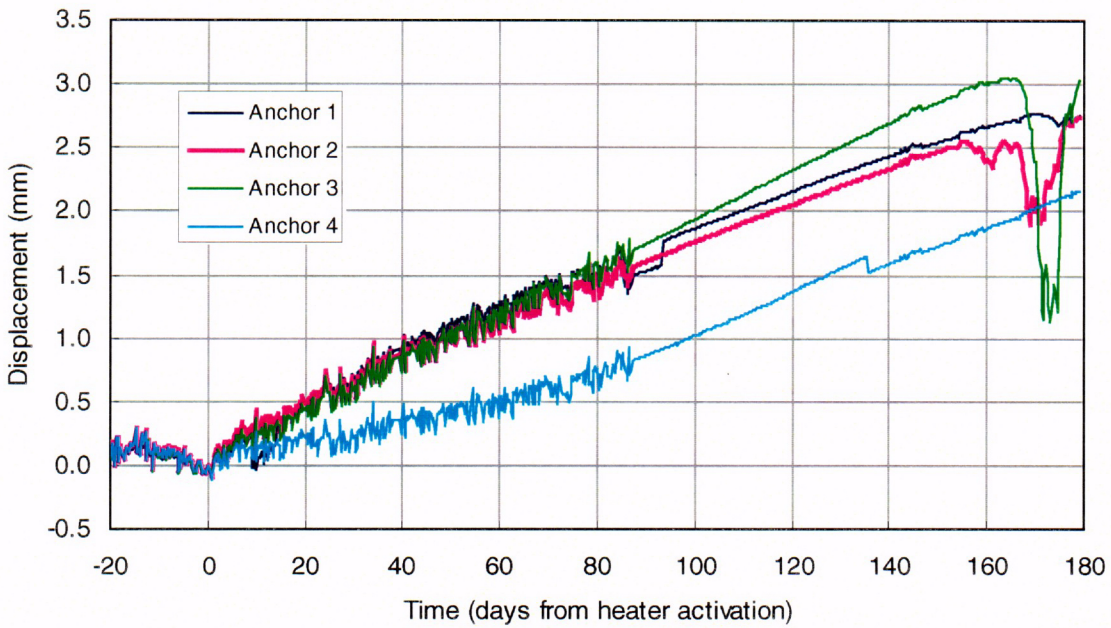


Figure 4-7. Measured displacements from ESF-HD-150-MPBX6 (corrected for thermal expansion).

C 34

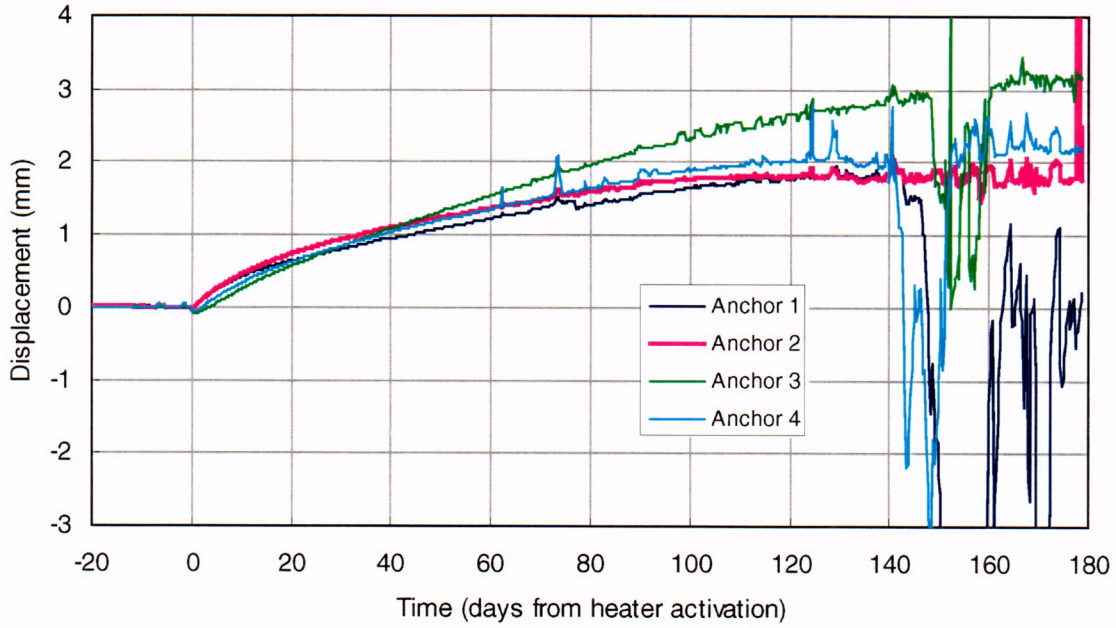


Figure 4-8. Measured displacements from ESF-HD-154-MPBX7 (corrected for thermal expansion).

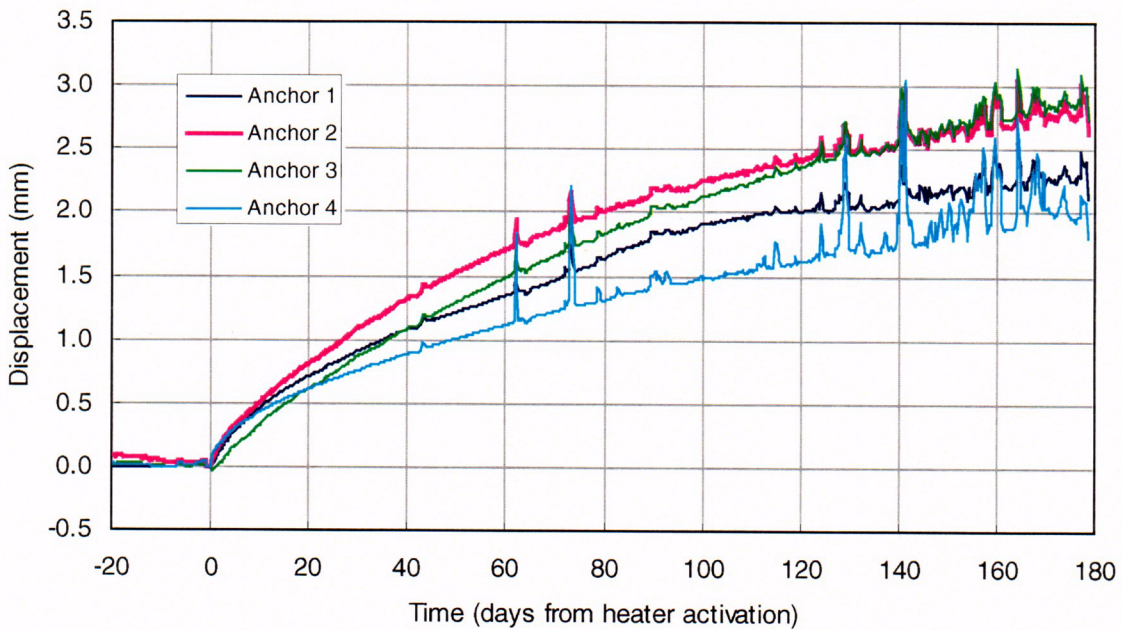


Figure 4-9. Measured displacements from ESF-HD-155-MPBX8 (corrected for thermal expansion).

C 35

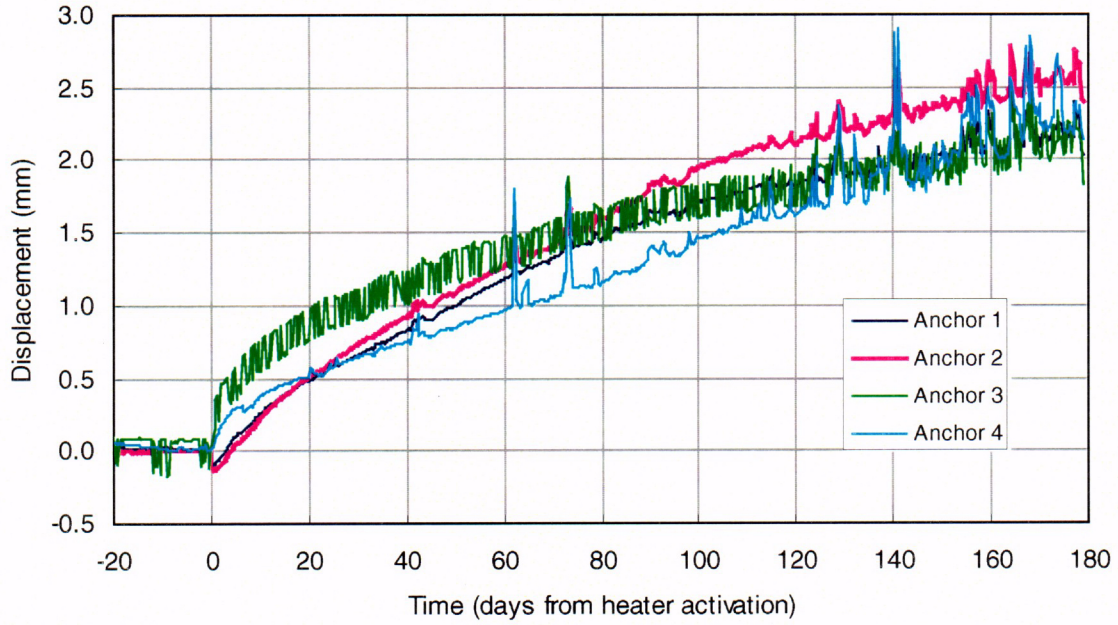


Figure 4-10. Measured displacements from ESF-HD-156-MPBX9 (corrected for thermal expansion).

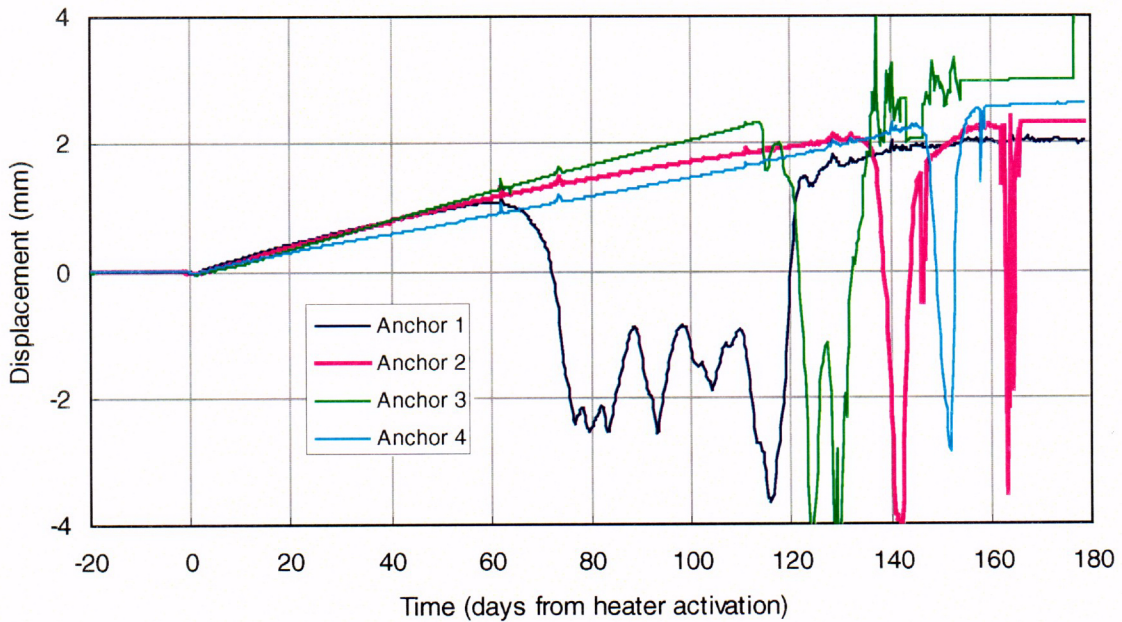


Figure 4-11. Measured displacements from ESF-HD-157-MPBX10 (corrected for thermal expansion).

C36

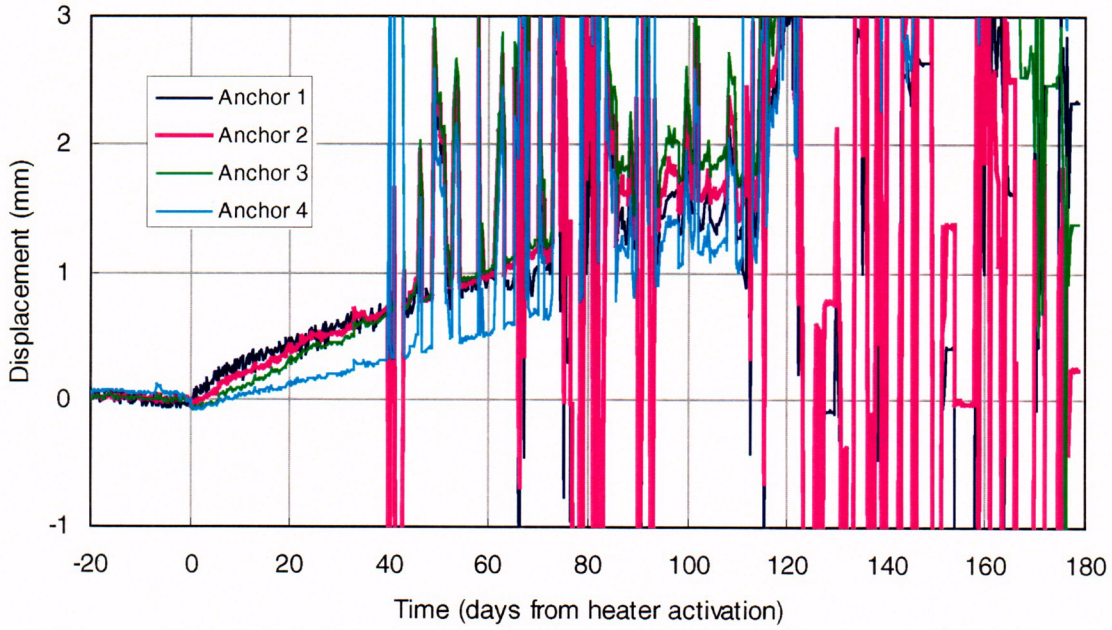


Figure 4-12. Measured displacements from ESF-HD-178-MPBX11 (corrected for thermal expansion).

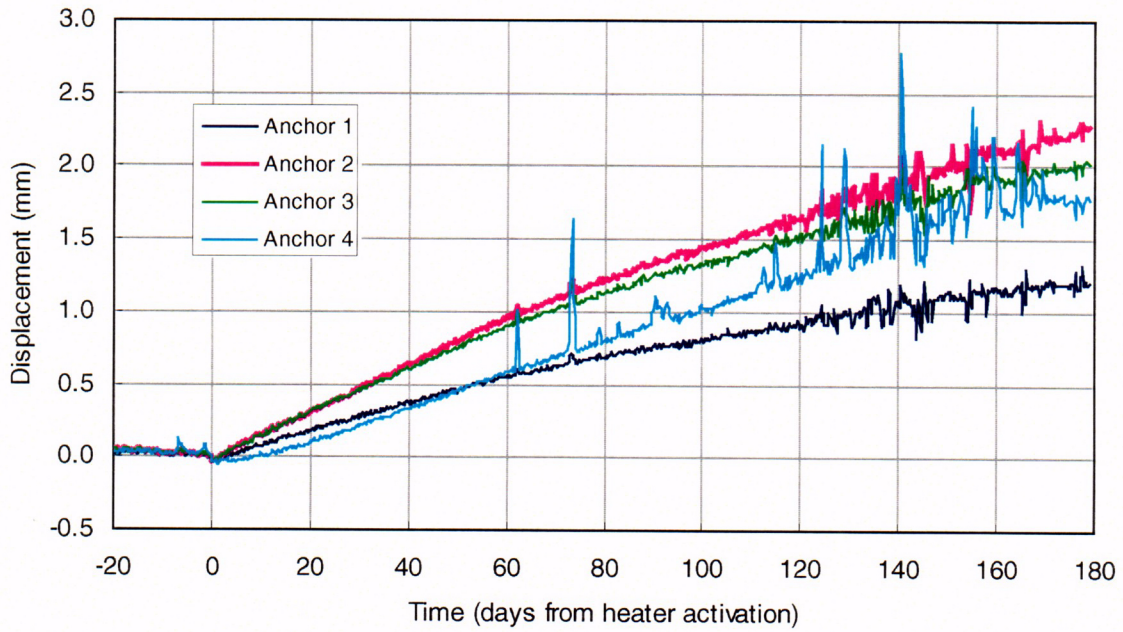


Figure 4-13. Measured displacements from ESF-HD-179-MPBX12 (corrected for thermal expansion).

C37

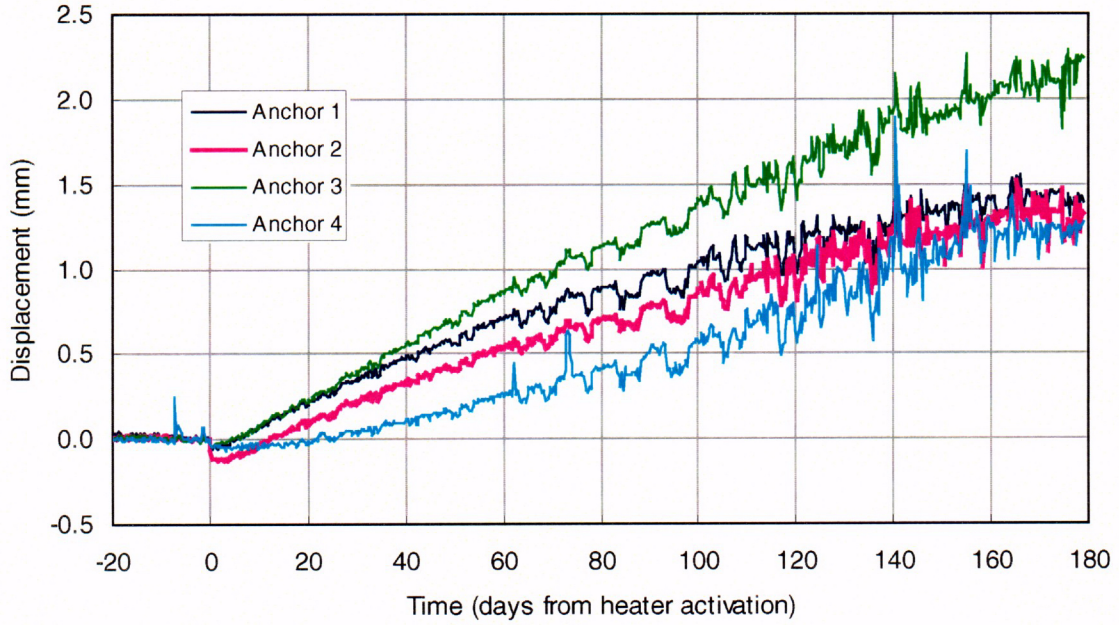


Figure 4-14. Measured displacements from ESF-HD-180-MPBX13 (corrected for thermal expansion).

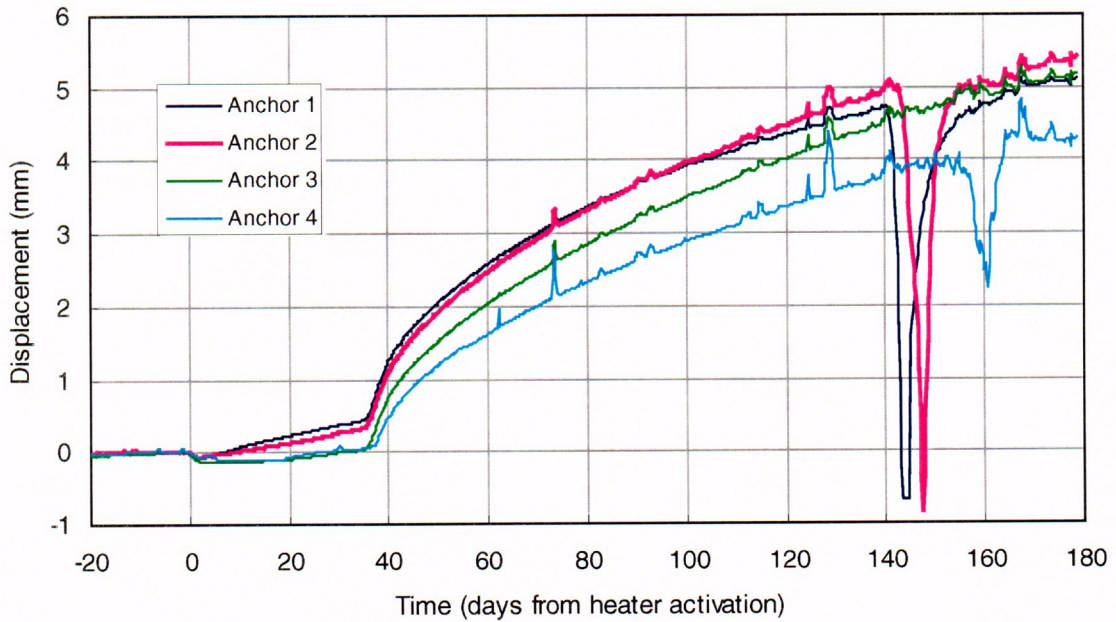


Figure 4-15. Measured displacements from ESF-HD-181-MPBX14 (corrected for thermal expansion).

C 38

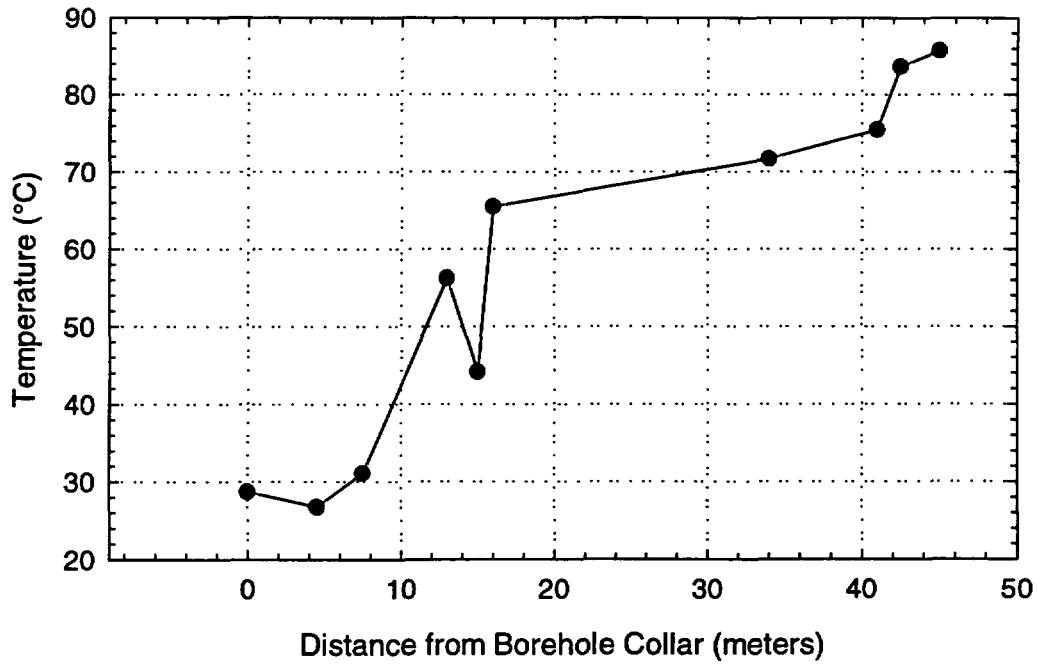


Figure 4-16. Measured temperatures from ESF-HD-81-MPBX1.

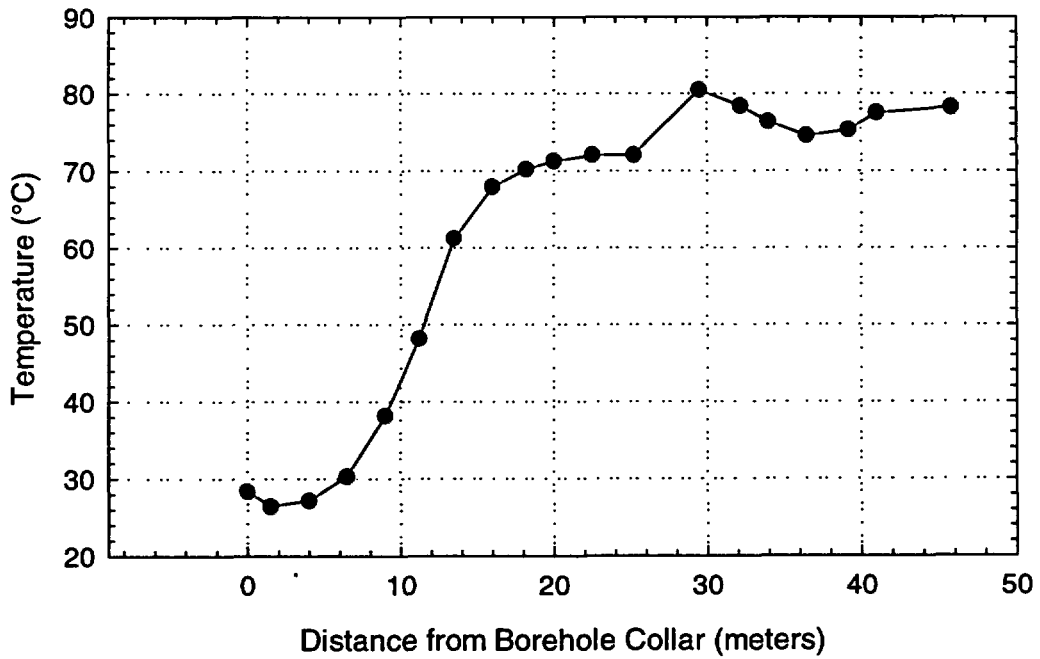


Figure 4-17. Measured temperatures from ESF-HD-82-MPBX2.

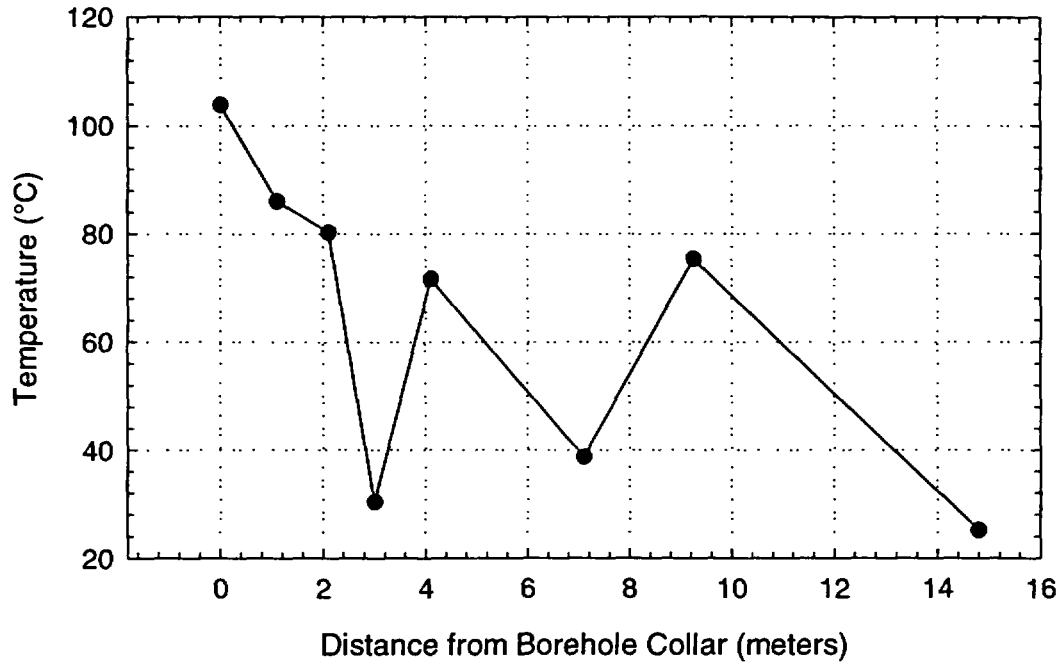


Figure 4-18. Measured temperatures from ESF-HD-147-MPBX3.

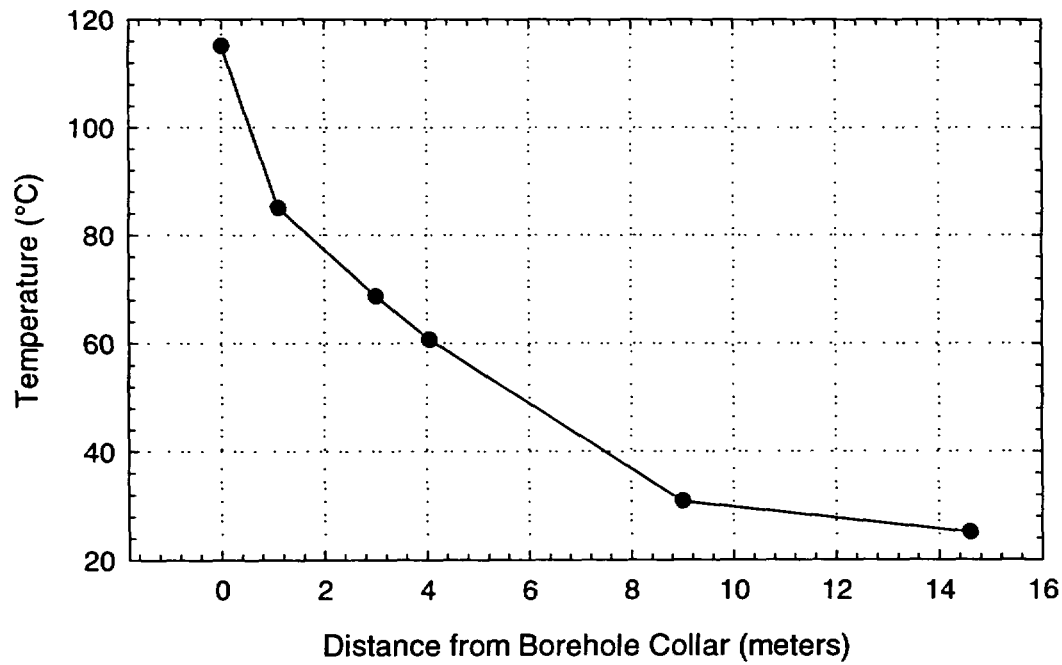


Figure 4-19. Measured temperatures from ESF-HD-148-MPBX4.

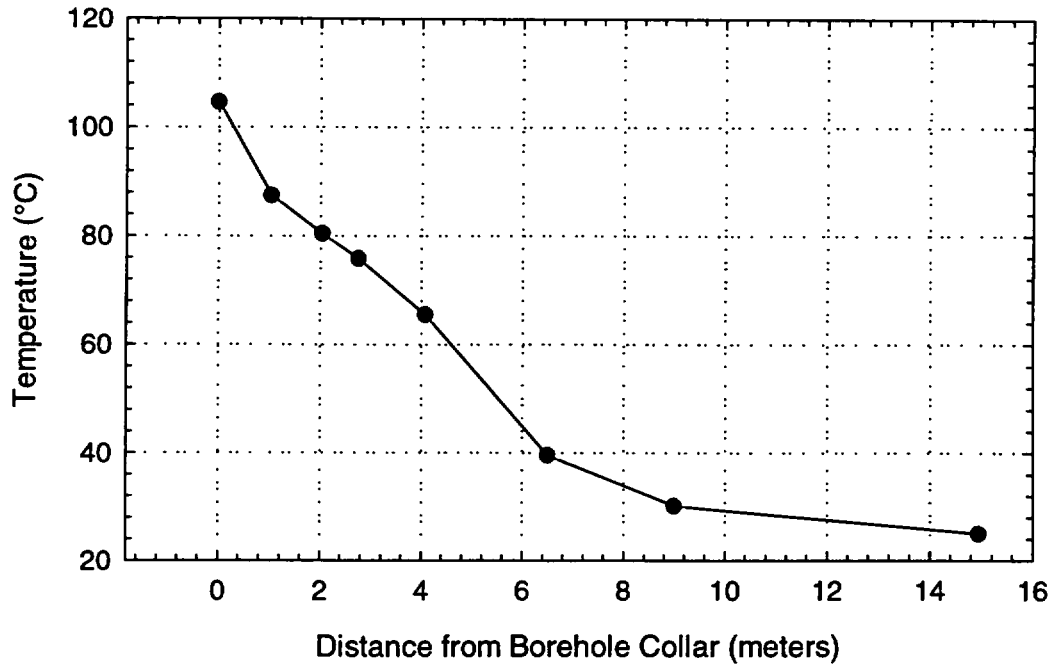


Figure 4-20. Measured temperatures from ESF-HD-149-MPBX5.

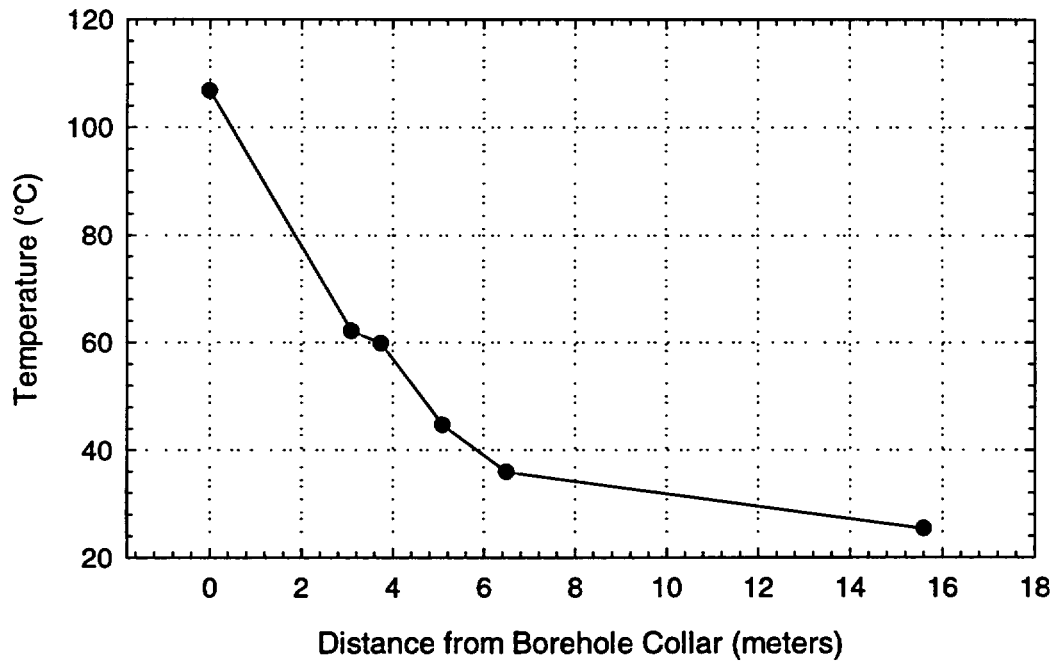


Figure 4-21. Measured temperatures from ESF-HD-150-MPBX6.

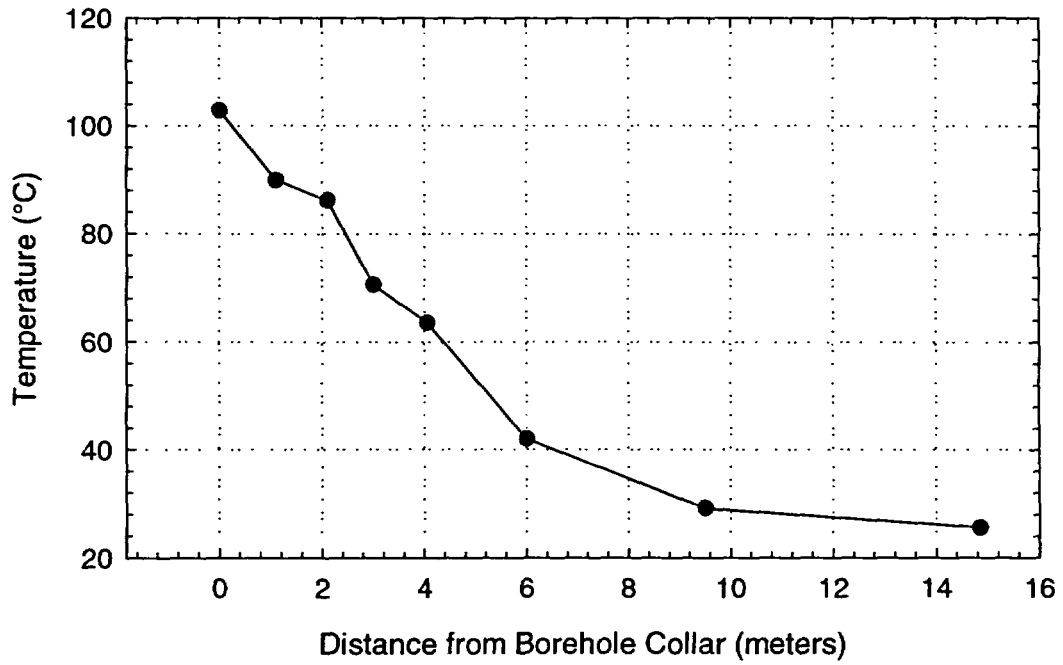


Figure 4-22. Measured temperatures from ESF-HD-154-MPBX7.

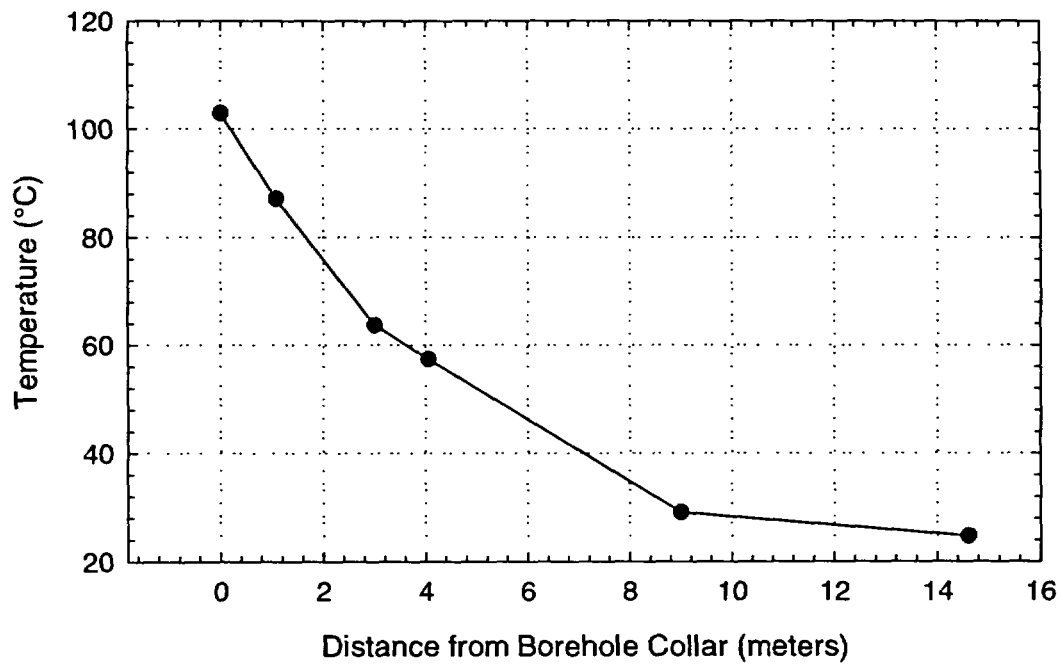


Figure 4-23. Measured temperatures from ESF-HD-155-MPBX8.

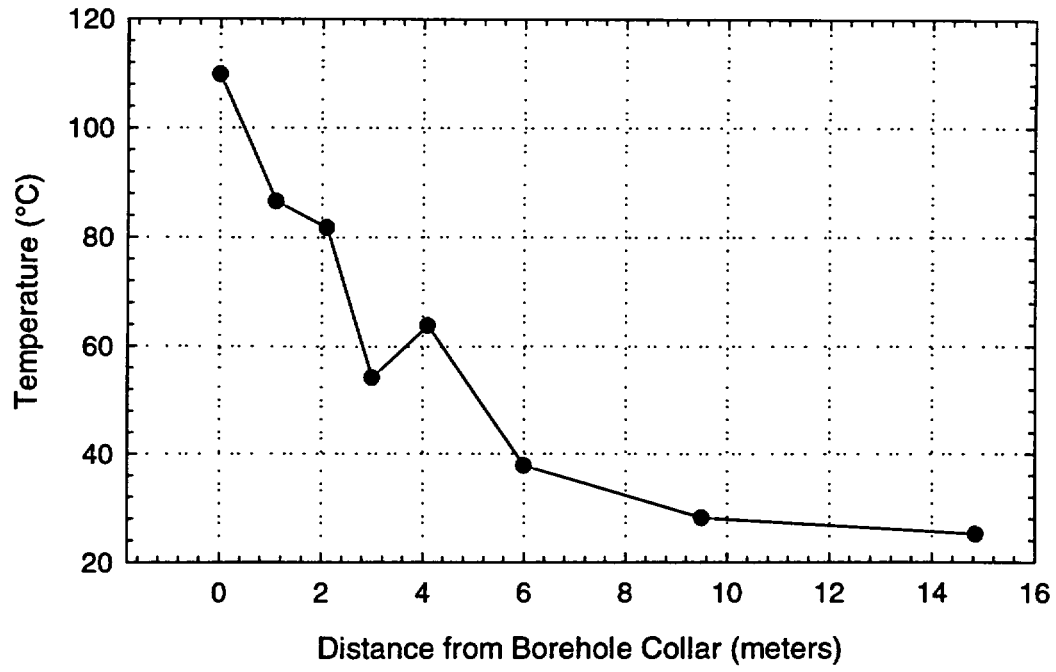


Figure 4-24. Measured temperatures from ESF-HD-156-MPBX9.

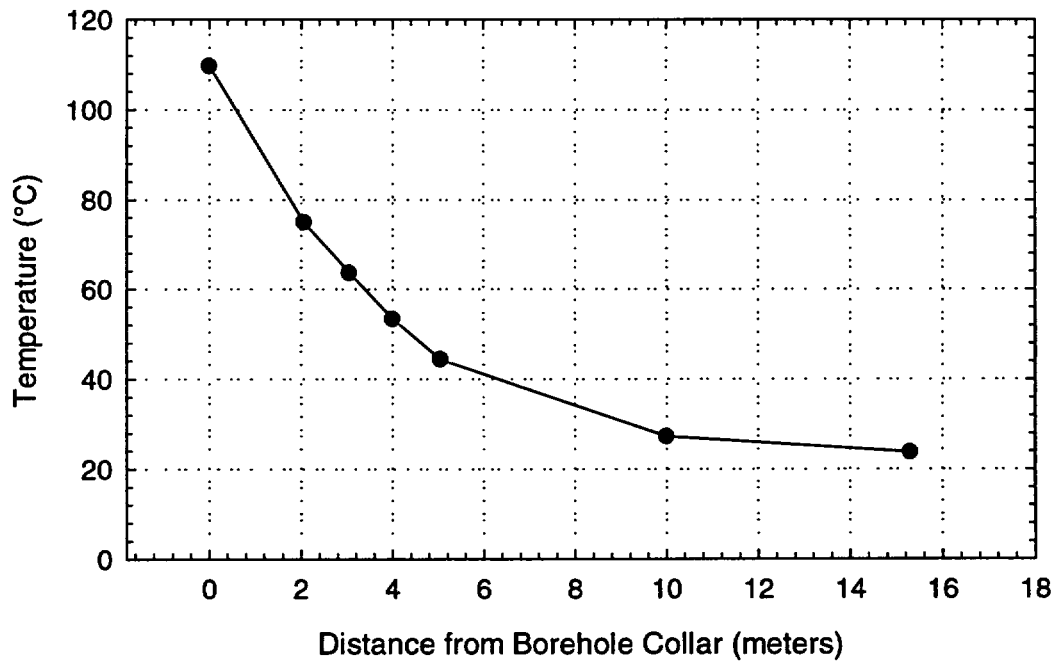


Figure 4-25. Measured temperatures from ESF-HD-157-MPBX10.

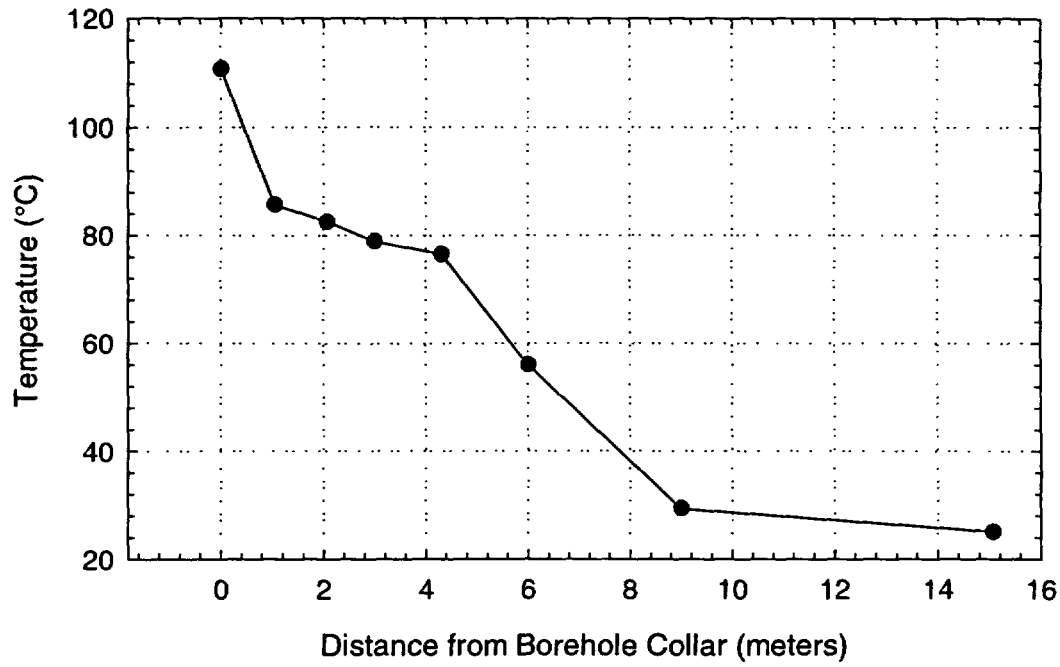


Figure 4-26. Measured temperatures from ESF-HD-178-MPBX11.

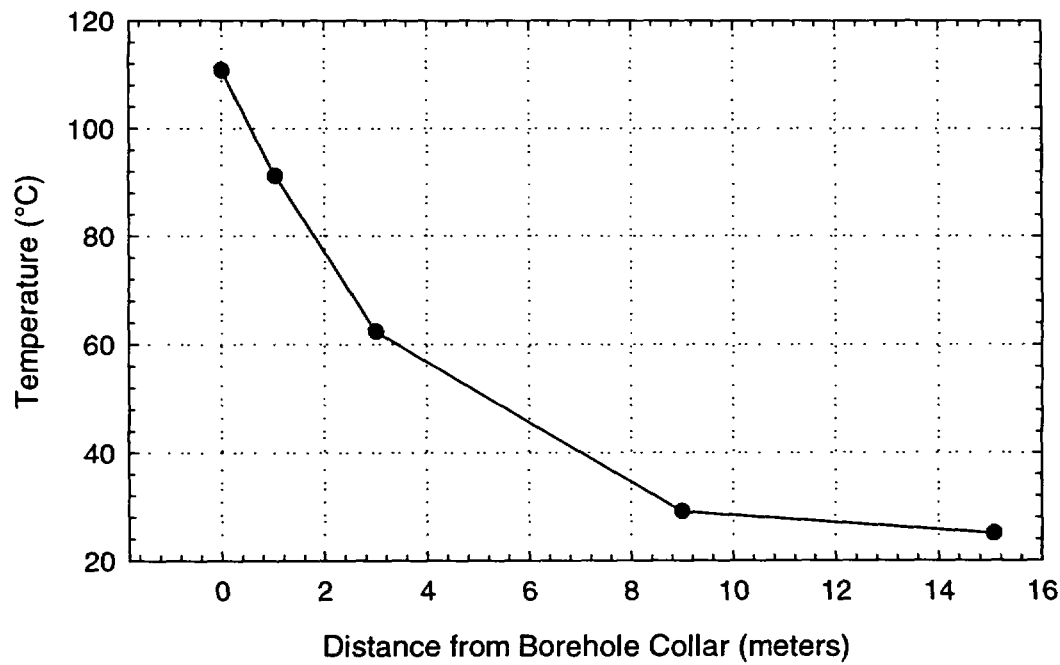


Figure 4-27. Measured temperatures from ESF-HD-179-MPBX12.

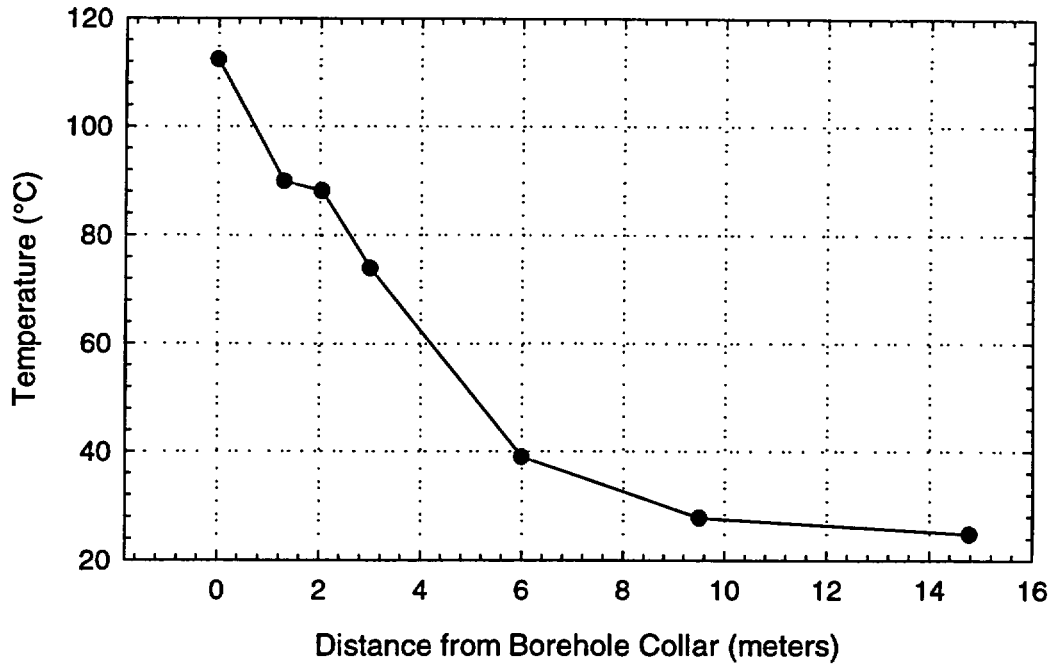


Figure 4-28. Measured temperatures from ESF-HD-180-MPBX13.

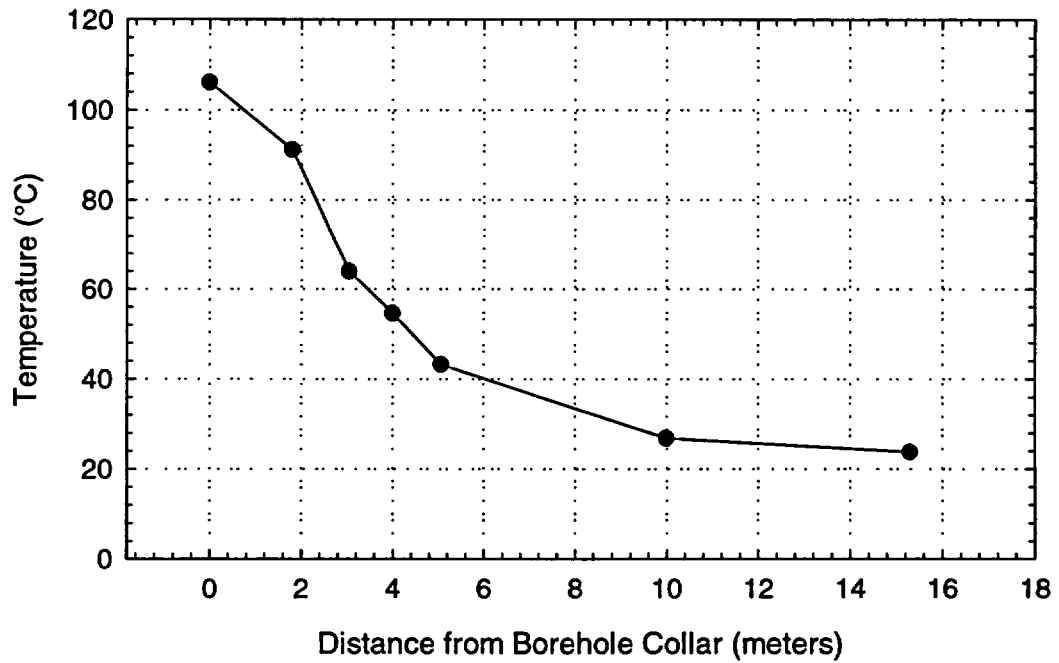


Figure 4-29. Measured temperatures from ESF-HD-181-MPBX14.

These figures show typical profiles with the highest temperature recorded at the MPBX head and the lowest temperatures at the bottom anchors, each located about 15 m from the borehole collar. The maximum temperatures through May 31, 1998 range from about 102° to 115°C with the highest collar temperatures exhibited in the MPBXs typically near the midpoint of the Heated Drift (MPBX7 through MPBX10). However, the single highest collar temperature is at the collar for MPBX4 (near the bulkhead), and the average temperature of the MPBX collars in the lined section (MPBX11 through 14) is slightly higher than at the midpoint at 179 days. The lower temperatures at the MPBXs nearest the bulkhead are likely due to subtleties in the overall temperature distribution associated with edge effects. The surface thermocouples in the lined section show lower temperatures than in the middle of the drift; it is unknown why the corresponding MPBX collar temperatures are slightly higher. Also, the collar temperatures for the vertically down MPBXs are consistently lower than their upward counterparts at each MPBX cross-section. This is likely due to the manner of MPBX head installation for these downward MPBXs. The heads were recessed into the concrete invert about 10 cm to minimize the construction and test installation interference. The associated temperature sensors are therefore slightly farther from the radiation heat transfer effects of the canister heaters and more strongly influenced by the conduction of the concrete than their upwardly installed counterparts which were located at the actual borehole collar. The general trend for all MPBX temperature measurements is exponentially decreasing with distance from the collar as should be expected. As discussed in Section 3 (see Figure 3-39) the temperature data in the MPBX boreholes in the Heated Drift experienced oscillations related to barometric pumping during the second quarter of the DST. These oscillations are seen in some of the displacement data as well. The data will continue to be evaluated in future DST reports.

The DST displacement data exhibited by the long lateral MPBXs (ESF-HD-MPBX1 and ESF-HD-MPBX2) presented in Figures 4-2 and 4-3 are consistent with expected displacement behavior throughout the period ending May 31, 1998. Both of these MPBXs exhibit limited compressional displacements during the very early heating periods, followed by general extension of the deepest anchors, and continued compression of the anchors nearest the collar. The initial compression is caused by the relatively small volume of rock heated during very early time periods, which tends to “push” the anchors toward the cool collar region. After a sufficient volume of rock is heated, the volumetric thermal expansion begins to “engulf” the deeper anchors, and causes a general lengthening of the entire gage length. Naturally, the anchors nearest the collar are the last to “feel” this effect, and continue with general compression throughout the reporting period. ESF-HD-MPBX-1 is installed in borehole #81 which is located on the northern side (right rib) and about 4.54 m from the HD. ESF-HD-MPBX2 is installed in borehole #82 which is located on the southern side and about 4.8 m from the HD. Interestingly, the displacements measured by ESF-HD-MPBX2 are somewhat higher (more extensional) than those from ESF-HD-MPBX1. In fact, the maximum extension measured by MPBX2 (Anchor 6, the deepest anchor) is about 40% higher than the equivalent measurement from MPBX1. It is possible MPBX2, which is located in the pillar separating the Heated Drift from the Observation Drift, is in rock that is less constrained than is MPBX1 which is located in rock not bounded by a similar opening. The results shown for both MPBX1 and MPBX2 are consistent with the pretest linear thermoelastic analyses conducted for the DST discussed in Francis et al. (1997). Additional discussion of these comparisons is given in Section 6 of this report.

The MPBXs installed within the Heated Drift and presented in Figures 4-4 through 4-15 show general closure of the Heated Drift after initiation of heating. The maximum magnitudes of closure (not counting the MPBXs in the invert) for each MPBX array range from about 2.9 mm vertically for MPBX3, located in the array nearest the bulkhead, through 3.1 mm for MPBX7, located in the middle array, to about 2.4 mm for MPBX12, located in the rear array in the CIP concrete section of the Heated Drift. Again, it is not surprising that the maximum displacements are measured near the Heated Drift midpoint as the rock mass in this vicinity is most greatly affected by the heating of the Heated Drift. Also, it is likely that the MPBX array located in the CIP section is somewhat constrained by both the CIP liner and by the slightly lower temperatures in this region (see Section 3). Likewise, the MPBX array nearest the thermal bulkhead is probably somewhat affected by the edge effects associated with being nearest the end of the Heated Drift. With the exception of data from a few gages that have obviously gone bad (all the gages for MPBX11, MPBX7-1, MPBX5-1 and 2), the data presented in Figures 4-4 through 4-15 are generally consistent with one another.

The data from some of the MPBXs appear to be affected by one of three types of "noise." One type is the classic cyclic noise, which may be due to the nearby presence of the wing heater power cables or some other electrical disturbance. It appears that for a number of gages, this noise begins around 120 to 130 days. There were several activities that began in the vicinity of the Heated Drift around that time: construction of concrete floors in the Observation and Connecting Drifts, insulation of said drifts, TBM mining of the ECRB drift (Enhanced Characterization of the Repository Block). It is currently unknown whether any of these activities may be related to the noise, but these possibilities are currently being evaluated. A second type of noise appears to be directly correlated to the apparent barometric pumping in the MPBX boreholes described in Section 3 (Figure 3-39). The raw, converted, and thermally corrected displacement data in some gages (e.g., MPBX3) undergo oscillations that correspond to the same behavior in the thermocouples in that borehole. A third noise, which is really an abnormality, is expressed in the data for MPBX6, MPBX7, MPBX10, and MPBX14. For several of the gages in these MPBXs, and at different times, the displacements inexplicably drop suddenly and drastically, then take several days to recover to a reading fit to the previous curve of the data. There is currently no explanation for this abnormality; hopefully this phenomenon will be explained in future DST data reports.

The first and second Heated Drift MPBX arrays are located approximately 13.7 m and 21.3 m from the thermal bulkhead respectively. Each of the upward MPBXs exhibits some initial compression as the heaters are initiated, with the most compression seen in MPBX4 located and oriented toward the north and MPBX9 located vertically up in the second array. A consistent theme with these measurements is that the deepest anchors (located 15 m from the Heated Drift) generally exhibit the least amount of displacement during this reporting period, and anchors nearer the collar exhibit greater displacements. This is consistent with the concept of volumetric thermal expansion with small volumes of rock heated near the Heated Drift during early time periods. Because only small volumes of rock are thermally expanding, there is little influence on the deepest anchors located 15 m away. The nearer anchors and the borehole collar are moving in opposite directions in a relative sense, with the nearest anchors being "pushed" into the rock mass relative to the deeper anchors. At later times, as increasingly larger volumes are affected, the traces of the deeper MPBX anchors cross those of the nearer ones, indicating that the thermal pulse has engulfed that region. It is expected that the anchor 4 data traces will eventually

overtake those of the other anchors and become the largest displacements. These results, like those of MPBX1 and MPBX2, are consistent with the pretest linear thermoelastic analyses performed by SNL prior to conducting the DST (Francis et al., 1997). Additional discussion of these pretest analyses and comparison to selected data are given in Section 6 of this report.

The final MPBX array is located approximately 39 m from the thermal bulkhead within the CIP concrete liner section of the Heated Drift. As suggested previously, the displacements from these MPBXs are generally smaller than similar measurements from the other MPBX arrays. This should not be unexpected as the CIP provides substantial support during early times and the edge effects reduce the temperatures in this region somewhat. The most interesting and significant observation from the MPBX data during this early time period is the results from MPBX14 (Figure 4-15) which show a marked increase in displacement rate after about day 35. The data trends are remarkably stable throughout the reporting period (with the exception of the abnormalities described earlier). MPBX14 is located in a borehole drilled vertically down through the concrete invert segment and the CIP liner. The anchors are all located in solid rock below the CIP liner at distances within the rock equivalent to the other MPBXs. It is important to note that the displacements exhibited by MPBX14 at early times show the largest displacements measured by anchor 1, followed by anchors 2, 3, and 4. This trend differs completely from the other MPBXs in which the intermediate anchors show the largest displacements during this early time period. A possible explanation for this behavior is that the invert segment is debonding from the underlying CIP concrete due to distortional displacement of the Heated Drift CIP liner. The magnitudes of displacements for MPBX14 are also much larger than for the other two MPBXs located in the invert in the unlined drift, MPBX6 and MPBX10. Detailed analyses of potential CIP liner behavior are discussed in Section 6.2.3. These analyses use the best available material properties and a refined mesh capable of discerning complex CIP behavior.

## **4.2 Displacement Measurements—Drift Closure**

Two cross-drift extensometers (CDEX) were installed within the cast-in-place (CIP) section of the DST to measure vertical and horizontal drift convergence. These convergence meters, which were conceived by SNL and designed and fabricated by GEOKON, consist of 5.68-meter long Invar rods connected to stainless steel pins mechanically anchored into the CIP liner at the inner surface of the liner and invert. A single high temperature LVDT was installed along the tensioned rods to measure diametrical changes in the CIP in both the vertical (ESF-HD-CDEX-1) and horizontal (ESF-HD-CDEX-2) orientations. Temperature compensation for rod thermal expansion effects was made using Type-K (chromel-alumel) mineral insulated/metallic sheathed ungrounded thermocouples. Ungrounded in this case refers to the thermocouple junction itself which is electrically insulated from the stainless steel sheath. The locations of the LVDTs and individual thermocouple junctions were determined from the survey coordinates and from the field notes for installation. The measured displacements were corrected for the thermal expansion of the Invar rods as described in Section 4.1.

The results of the horizontal and vertical CDEXs are shown in Figure 4-30. The horizontal CDEX displays an immediate and relatively large amount of compression as the wing heaters energize a large region of rock at the ribs, causing significant thermal expansion toward the drift opening. Because the wing heaters heat a large volume of rock in the ribs of the Heated Drift, horizontal stresses there will increase relative to the vertical stress.

This increased thermally induced horizontal stress will “ovalize” the Heated Drift, or shorten the horizontal diameter of the Heated Drift relative to the vertical, as illustrated by the vertical CDEX data. Around 35 days, however, the slope of the vertical CDEX data changes from positive to negative, indicating other phenomena are causing the Invar rods to move back towards the drift opening. At about 160 days, the vertical CDEX begins to measure net compression. At least two phenomena may be contributing to this change. One, the rock surrounding the tunnel may have undergone a sufficient thermal input by that time to heat and expand a volume of rock capable of compensating for the rock mass movement due to stress-induced ovalizing of the drift. Two, the unusual data from MPBX14 (Figure 4-15, Section 4.1) show a marked increase in the displacement rate at the invert after about day 35 after heating. A possible explanation for this behavior is that the invert segment is debonding from the underlying CIP concrete due to distortional displacement of the Heated Drift CIP liner. The behavior exhibited by the combination of the CDEXs and MPBX14, along with that of the strain gages described in Section 4.4, is very complex in nature; additional discussion and modeling of this behavior and comparison to pretest analyses are given in Section 6 of this report.

One other observation regarding the CDEX data is the noticeable increase in noise beginning on about day 135. These data correspond to noise increases in many of the MPBXs and strain gages, and they appear to correlate with some discrete event or activity in the vicinity of the Heated Drift.

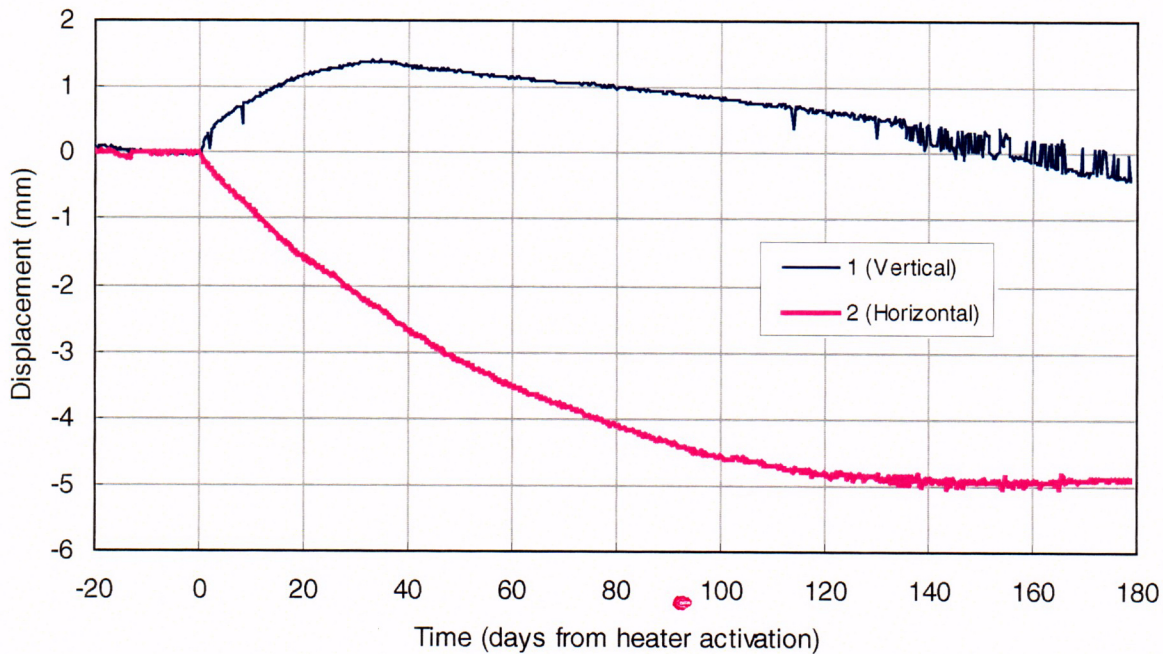


Figure 4-30. Measured displacements from the cross-drift convergence gages (corrected for thermal expansion).

C39

### 4.3 Displacement Measurements—Sequential Drift Mining Gages

This section contains information for Sequential Drift Mine-by (SDM) Experiment MPBXs (ESF-SDM-42-MPBX1, ESF-SDM-43-MPBX2, and ESF-SDM-44-MPBX3) located in the Observation Drift. The SDM Experiment is a two-phased experiment. The first phase involves monitoring the rock response as result of the sequential mining of the Heated Drift. This phase includes the initial mining by the Alpine Miner (December 3, 1996 to January 16, 1997) and the invert removal by blasting (January 21, 1997 to February 6, 1997), followed by the long-term ambient behavior until the heaters were turned on (December 3, 1997). The second phase involves monitoring the rock response as a result of heating in the Heated Drift Test. This phase includes heater activation (December 3, 1997) through the reporting period (May 31, 1998).

Three MPBXs were installed in November-December 1996 in boreholes 42, 43, and 44 drilled slightly downward from the Observation Drift toward the Heated Drift. Boreholes 42, 43, and 44 are located at Heated Drift stations 0+13.7, 0+20.8, and 0+32.2 m, respectively (each station refers to the y-axis distance from the Heated Drift bulkhead; see Figures 2-1 and 2-3). The boreholes were drilled wet using an NWX bit (7.57 cm diameter). They were each instrumented with GEOKON C-ring six-anchor MPBXs. Each of the C-ring anchors was connected to a Delrin MPBX head (located at the borehole collar) via Invar and carbon fiber connecting rods. During instrument installation in boreholes 42 and 44, the boreholes were sealed using aluminum tubing coated with Teflon. Aluminum tube was not used in borehole 43 as the hole was grouted and redrilled. All anchors and centralizers were electrically isolated from the rock using a Teflon coating. The MPBXs are a nominal 25 meters long and extend downward at an angle of approximately 10–11° to come within approximately 2 m of the Heated Drift left rib. The installed MPBXs have six anchors and five centralizers with the anchors set at approximately 16, 18, 20, 22, 23/24, and 25 meters from the head. Invar rods (in the anchor section, ~25 m to 16 m) and carbon fiber rods (in the centralizer section, ~16 m to head) are attached to each anchor and extend to the MPBX head. A vibrating wire displacement transducer is attached to each connecting rod to measure the relative displacement between the anchors and MPBX head which is fixed and sealed into the borehole collar. Temperature measurements are made along the lengths of each MPBX to provide temperature compensation for rod thermal expansion effects using Type-K (chromel-alumel) mineral insulated/metallic sheathed ungrounded thermocouples. Ungrounded in this case refers to the thermocouple junction itself which is electrically insulated from the stainless steel sheath. The locations of the anchors and individual thermocouple junctions were determined from the survey and borehole collar coordinates, from the field notes for installation (e.g., installed depth to various anchors and points on the MPBXs), and from manufacturers' and SNL specifications for the MPBXs.

The convention for the numbering of the anchors for the SDM MPBXs differs from the Heated Drift MPBXs. For the SDM boreholes, anchor number 1 is the farthest from the collar of the borehole (and the closest to the Heated Drift wall); anchor number 6 is closest to the collar. Table C-3 list the coordinates of the SDM MPBX anchors based on the Heated Drift coordinate system.

As stated above, the first phase of the Sequential Drift Mine-by Experiment involves monitoring the rock response as result of mining the Heated Drift. Collection of rock displacement data began on November 23, 1996 for ESF-SDM-42-MPBX1 and on December 20, 1996 for ESF-SDM-43-MPBX2 and ESF-SDM-44-MPBX3. Table 4-2 lists the dates the mining activities

passed by a given MPBX station. Mining activities for the Heated Drift included the initial mining by the Alpine Miner (December 3, 1996 to January 16, 1997) and the invert removal by blasting (January 21, 1997 to February 6, 1997).

Table 4-2. Heated Drift Mining Activities at SDM MPBX Stations

MPBX ID	HD Station	Alpine Miner at Station	Invert Blasting at Station
ESF-SDM-42-MPBX1	0+13.7 m	12/17/96 (352 days before DST)	1/24/97 (313 days before DST)
ESF-SDM-43-MPBX2	0+20.8 m	12/21/96 (348 days before DST)	1/29/97 (308 days before DST)
ESF-SDM-44-MPBX3	0+32.2 m	1/6/97 (331 days before DST)	2/4/97 (302 days before DST)

Figures 4-31 through 4-33 show the time history of anchor displacement from connection time for each MPBX (used as the reference time) up until heater activation (December 3, 1997). Note the six dashed vertical lines on these plots; these lines correspond to the chronological order of the six mining and blasting events outlined in Table 4-2. Also note that the displacements have been referenced to the first time at which data readings were taken for each vibrating wire transducer. The displacements shown after heater activation (t=0) in Figures 4-31 through 4-33 have not been corrected for thermal expansion of the Invar and carbon fiber rods; that correction will be added in later figures.

Figure 4-31 shows that all the anchors for SDM-MPBX1 were in an extension mode before heater activation, i.e., moving away from the head. This is the expected behavior for a converging mined drift. The displacements for the anchors on SDM-MPBX1 range from 0.08-0.25 mm right before heater activation. Also, the rank order of magnitude of displacement does not correspond to the numerical order of the anchors. Figure 4-32 shows for SDM-MPBX2 that only anchor 6 was in an extension mode with a jump that appears to be associated with invert blasting. The remaining five anchors appear to be in a compression mode with displacements ranging from -0.10 to -0.25 mm. Figure 4-33 shows for SDM-MPBX3 that all the anchors were in a compression mode, with two distinct discontinuities. This MPBX is exposed near the Observation Drift invert and the discontinuities may have been caused by construction activities in the Observation Drift. The displacements for these anchors range from -0.10 to -0.25 mm right before heater activation. The reason for the compression mode cannot be explained at this time; however, it should be noted that the displacements appear to be very small in comparison to those expected to be induced by heating. Explanation for the total extension observed along SDM-MPBX1 and the total compression observed along SDM-MPBX3 is not apparent at this time. Factors which may contribute to the observed behaviors include the proximity of MPBX1 to the connecting drift, the presence of the liner in the west end of the Heated Drift near SDM-MPBX-3, heating of the Heated Drift during DST installation, and possible undocumented collisions by test personnel into MPBX heads in the Observation Drift. Future analysis and computer modeling of the drift will help develop an explanation of these observed phenomena.

The second phase of the Sequential Drift Mine-by Experiment involves monitoring the rock response as result of the heated canister and wing heaters in the Heated Drift. Figures 4-34 through 4-36 show the time history of anchor displacement for SDM-MPBX1, 2, and 3, respectively, from heater activation (December 3, 1997) through the reporting period (May 31, 1998).

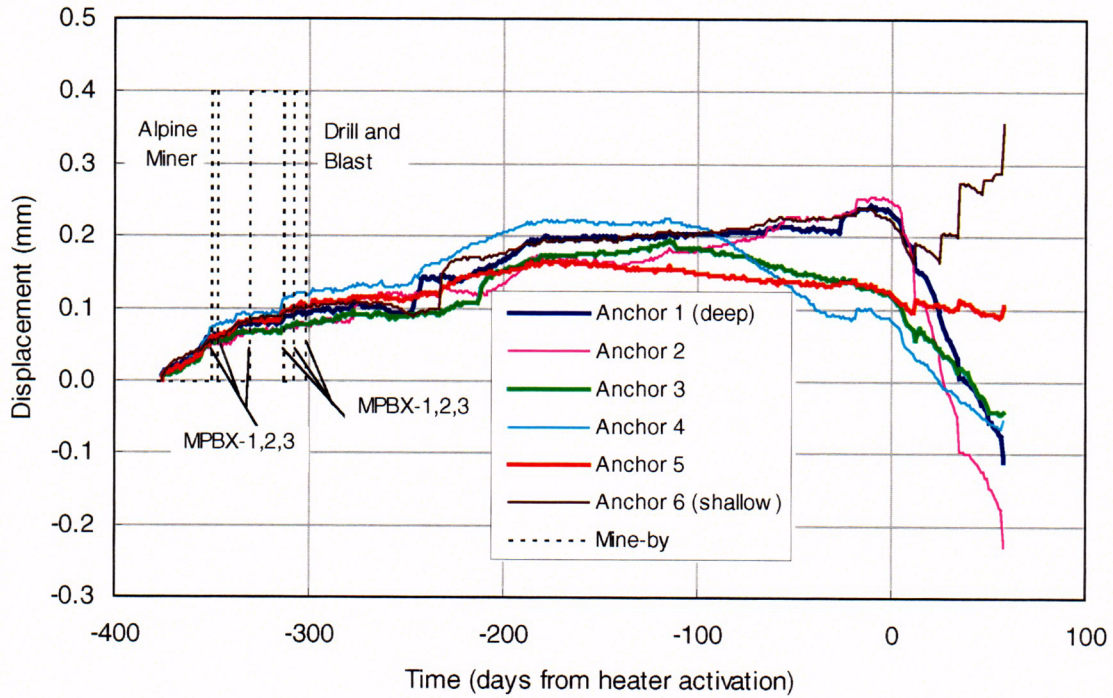


Figure 4-31. Measured displacements from ESF-SDM-42-MPBX1 (mine-by monitoring).

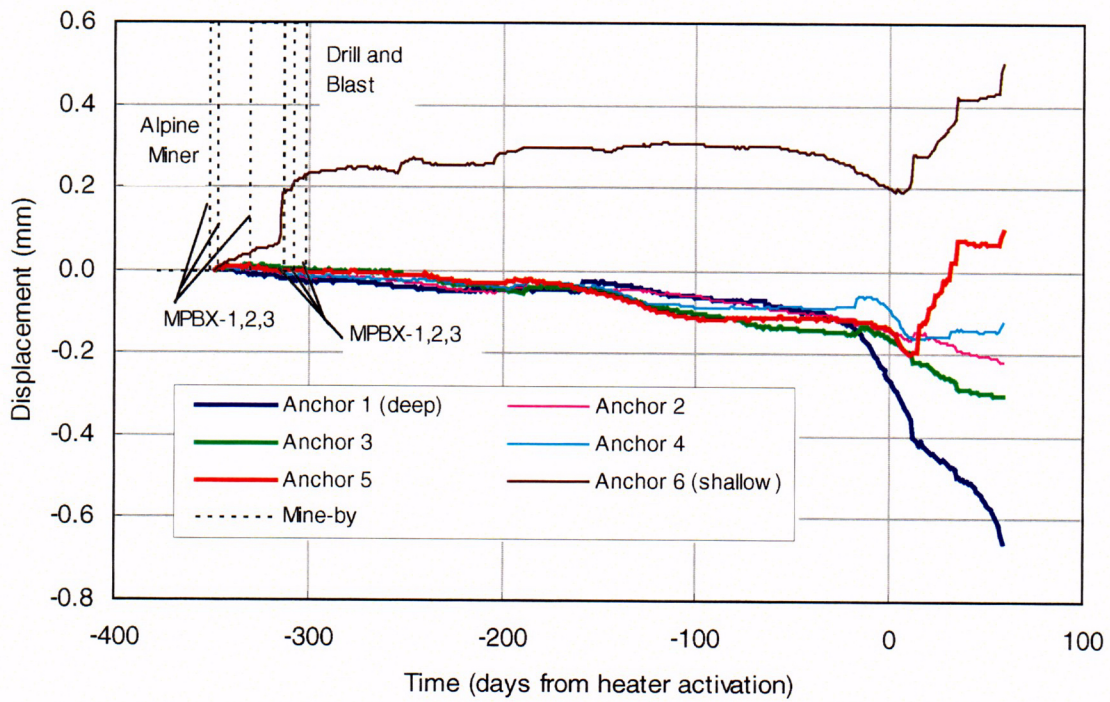


Figure 4-32. Measured displacements from ESF-SDM-43-MPBX2 (mine-by monitoring).

C40

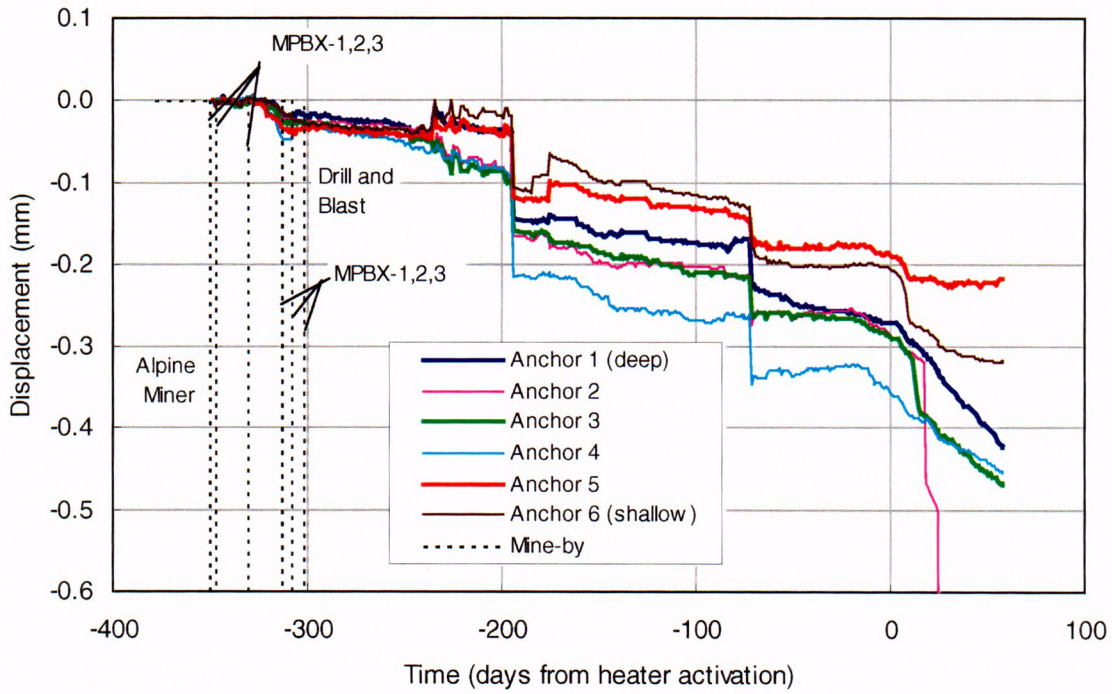


Figure 4-33. Measured displacements from ESF-SDM-44-MPBX3 (mine-by monitoring).

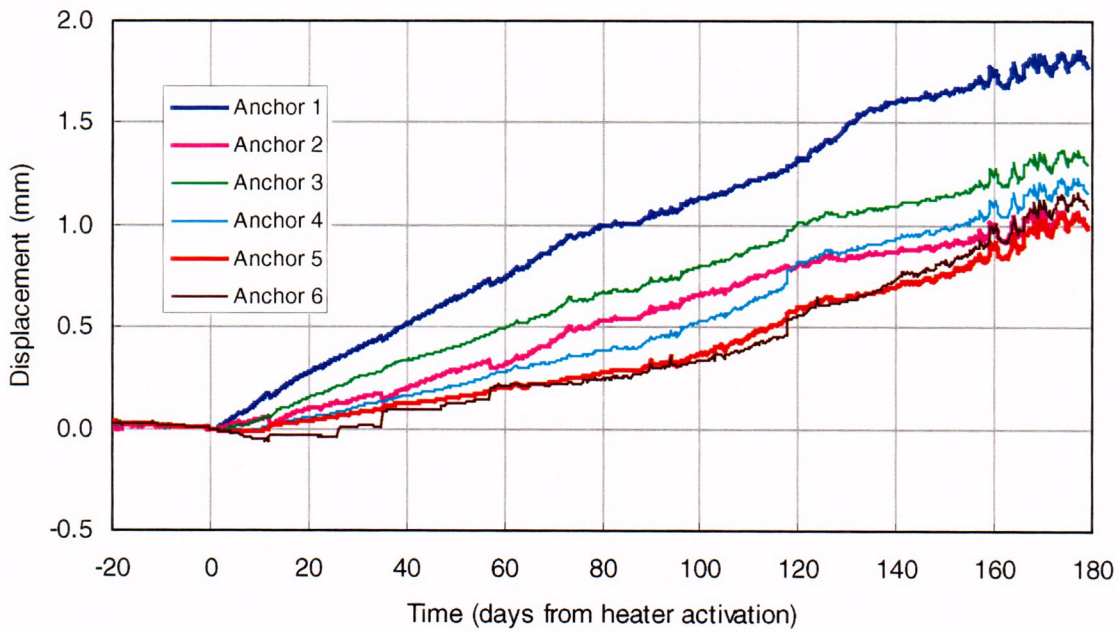


Figure 4-34. Measured displacements from ESF-SDM-42-MPBX1 (corrected for thermal expansion).

C41

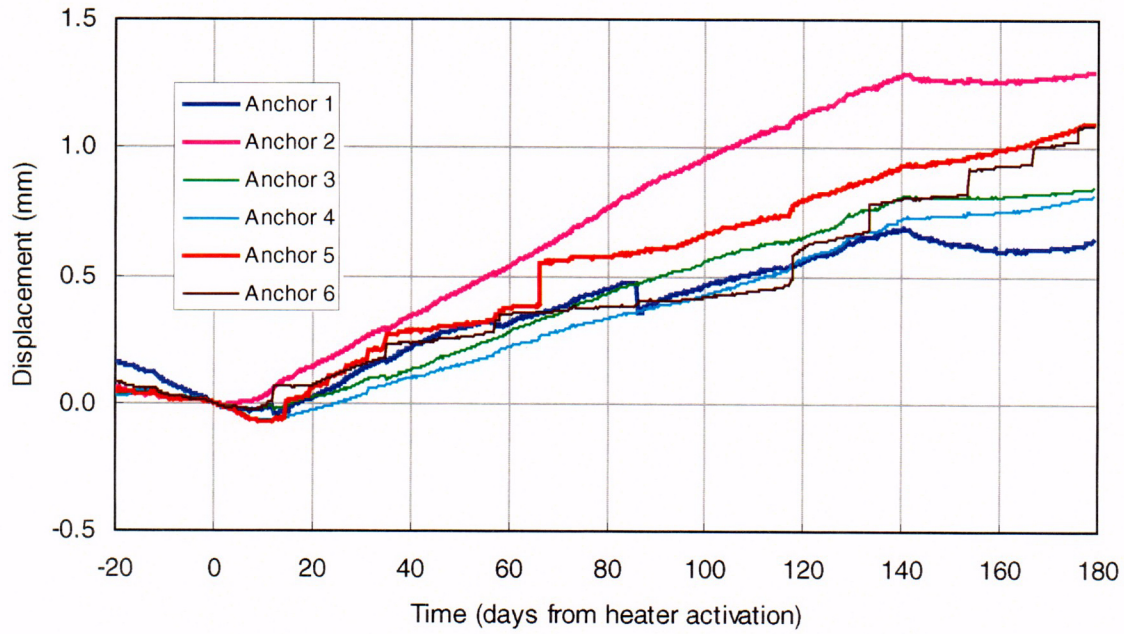


Figure 4-35. Measured displacements from ESF-SDM-43-MPBX2 (corrected for thermal expansion).

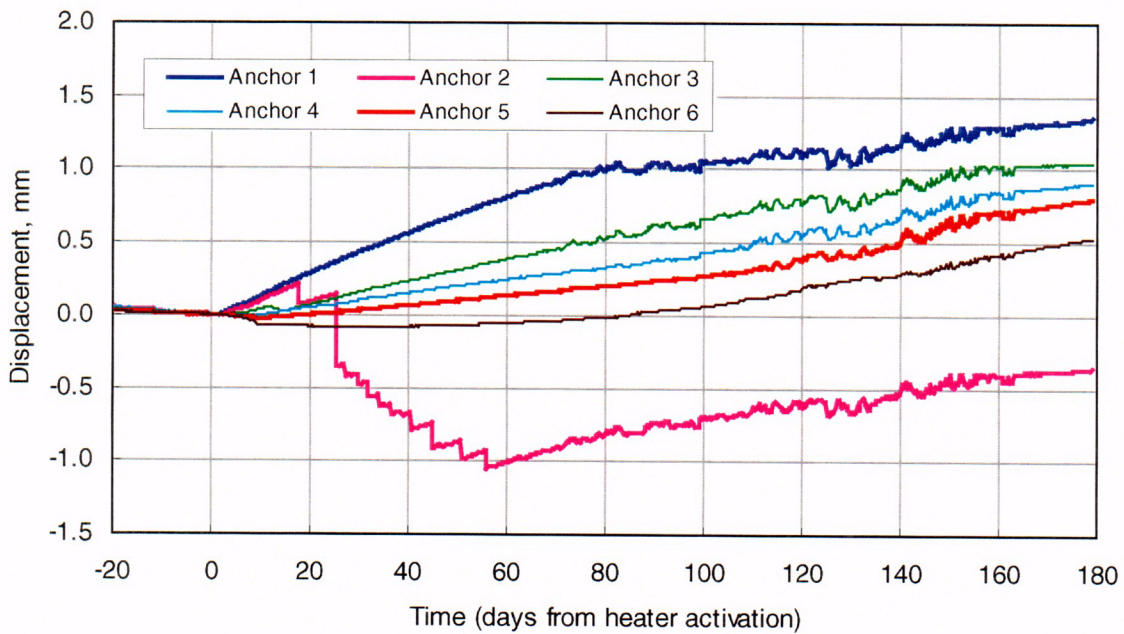


Figure 4-36. Measured displacements from ESF-SDM-44-MPBX3 (corrected for thermal expansion).

C42

For these figures, a correction has been added for the apparent displacement associated with the thermal expansion of the Invar and carbon fiber rods. This thermal correction has been performed in the manner described in Section 4.1. The thermal expansion coefficient of carbon fiber rod is  $1.48 \times 10^{-6}/^{\circ}\text{C}$  (data from GEOKON; see SNL, 1998). Also, the displacements in Figures 4-34 through 4-36 have been referenced to heater activation to highlight the effects of the heat input on the mechanical behavior of the rock mass.

Figures 4-34 through 4-36 show the anchors to be primarily in an extension mode, i.e., moving away from the head. The only exceptions to this are at early time for some of the deepest anchors for the SDM gages, where an initial "bunching up" of the anchors towards the collars is occurring. This behavior is much like that predicted and measured for the MPBX perpendicular to the heater in the Single Heater Test (SNL, 1998). SDM-MPBX 1 and 3 have very similar patterns of behavior, whereas SDM-MPBX2 is quite different. Typically for SDM-MPBX1 and 3 (Figures 4-34 and 4-36), anchor 1 (the anchor closest to the Heated Drift wall) shows the greatest extension, resulting from rock expansion into the Heated Drift driven by the nearby wing heaters. Anchor 6 for these MPBXs (the closest to the collar, and near the deepest end of the wing heaters) typically shows near-zero displacement, starting negative and slowly becoming positive. The magnitudes of displacements for the other anchors are approximately in rank order by anchor placement, although anchor 2 is out of order for both MPBX1 and 3. For MPBX2 (Figure 4-35), the rank order of magnitudes does not correspond to the order of the anchors, and peculiar behavior is seen for some anchors, particularly anchor 5. The cause of this erratic behavior, whether due to real phenomena in the rock mass or to some sort of gage failure, is not known at this time.

#### 4.4 Strain Gages

This section of this report completely supersedes the corresponding Section 4.4 in the 1st Quarter DST Data Report issued in April 1998 (DTN: SNF39012298002.001, TDIF #306771). Since the issue of that report, additional insight has been gained into the thermal correction of the strain measurements, which has produced significantly different results (although the conclusions from the strain gage data are essentially the same as in April).

The cast-in-place (CIP) concrete sections located at the west end of the Heated Drift were instrumented to monitor the concrete behavior during heating and cooling of the DST. The CIP liner was installed over approximately the final 12 m of the Heated Drift. Of this 12-m length, two different types of concrete were installed. The first four meters of the CIP (approximately 36-40 m from the bulkhead) consisted of the fiber reinforced concrete, and the final eight meters (approximately 40-48 m from the bulkhead) consisted of standard concrete. The thickness of the CIP is nominally 0.3 m, although the exact thickness is dependent on the mined surface roughness of the rock. A total of 45 four-inch-long Karma foil resistive strain gages was installed in 15 rosettes (three gages per rosette) in a circumferential-axial- $45^{\circ}$  pattern. The rosette layout is illustrated in Figure 4-37. Five rosettes were installed at each of three cross-sections equally spaced along the concrete section length. The three axial stations in the Heated Drift where the rosettes were installed are nominally  $y=37$ , 41.7, and 44.5 m; exact locations are presented in Table C-4. These cross-sections correspond roughly to the midpoint of the fiber-reinforced CIP liner section, and the third-points of the standard CIP section. The five strain gage rosettes at each station were located at the crown, left and right above the springline, and left and right near the concrete invert; this layout of the rosette locations is shown in Figure 4-38. The rosette strain

gages (RSG) are designated by rosette number and orientation (AXL=axial, CIR=circumferential, DIA=diagonal); for example, ESF-HD-RSG-5-AXL is the axial strain gage for rosette number 5. Although each rosette was originally intended to include three gages, some individual gages were damaged during installation, and others are producing what is considered suspect data. As of this report, 14 of the original 45 strain gages mounted on the inner surface of the CIP liner were not connected, have failed or are suspect. The gage failures are likely due to installation problems and/or bonding problems. Because of these failures, not all rosette locations have completely operational 3-gage rosettes. A complete list of failed and/or suspect gages is given in Section 5 of this report.

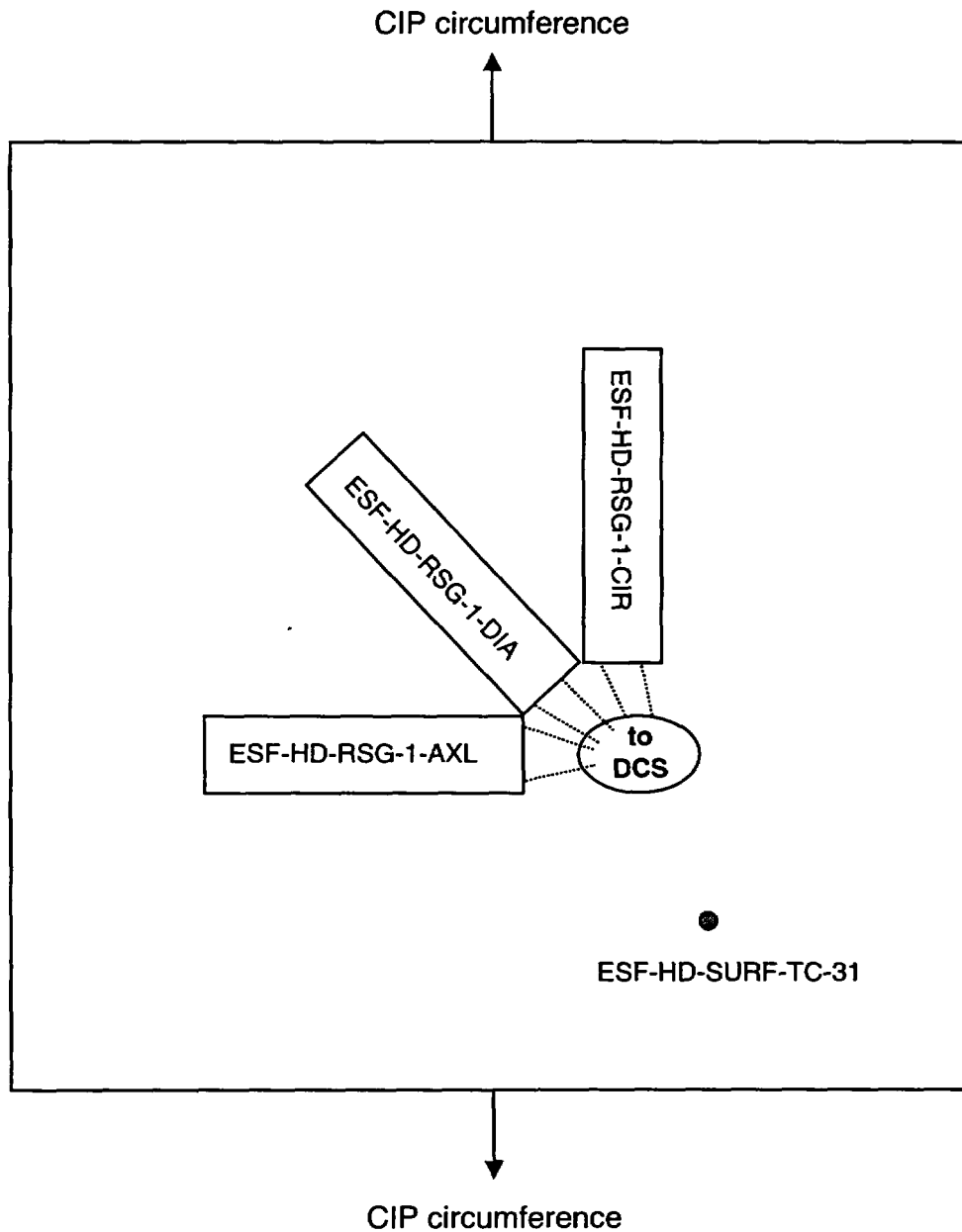


Figure 4-37. Layout of strain gages in rosette pattern.

### View Looking from Bulkhead

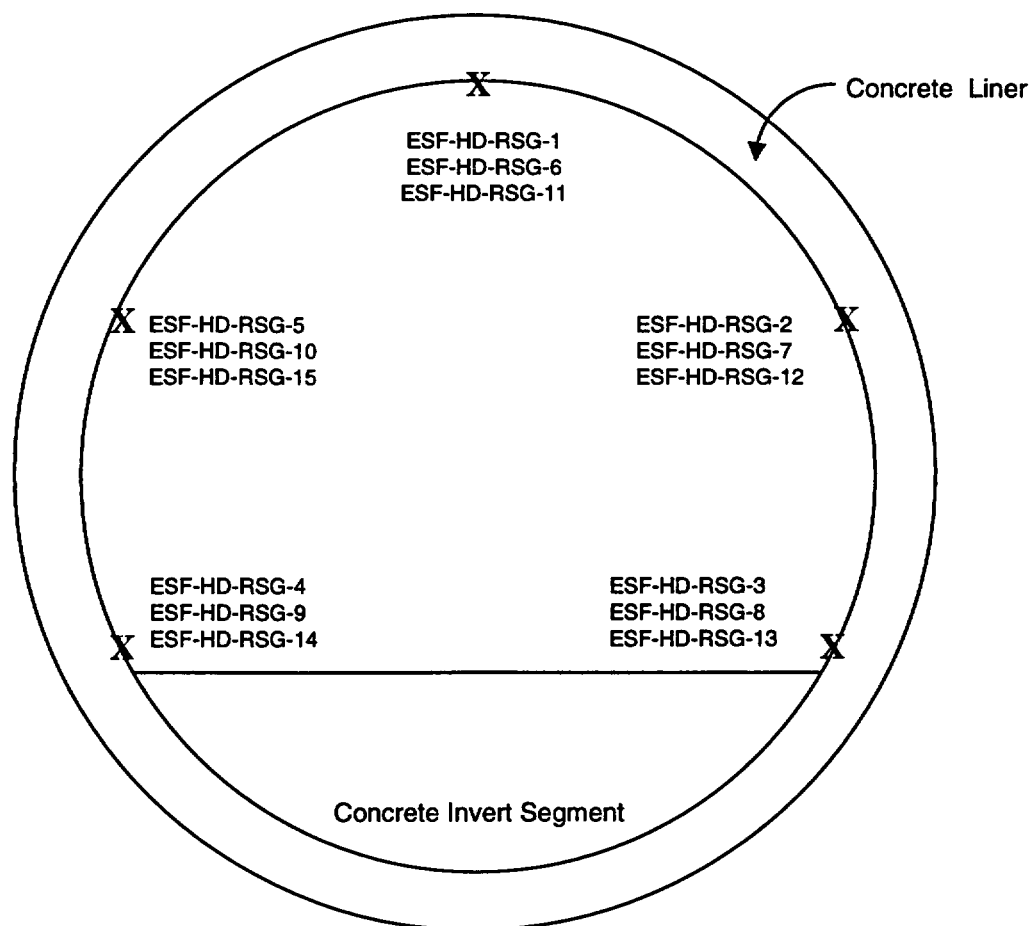


Figure 4-38. Location of strain gage rosettes on the concrete liner.

The strain gages were manufactured by BLH Electronics and installed by SNL. The gages were installed by carefully preparing the inner surface of the CIP liner using a Flexgrinder. Each gage was bonded to the prepared surface using a high temperature filled epoxy that was cured at approximately 250°C. Strain gage extension leads were fabricated using #32 AWG Teflon (PTFE) insulated triplex ribbon and/or twisted wire. Continuous strain gage/extension wire combinations using lead lengths up to 92 meters were installed to mitigate downhole connection uncertainties between gages and wire. Measured strains were corrected for thermal effects on the strain gage itself using an temperature-correction equation and constants supplied by the manufacturer. An additional thermal correction due to the thermal expansion of the temperature-compensated strain gages was also required.

Gage and anchor locations (as-builts) for strain gage measurements made for the DST are presented in detail in Appendix C of this report and additional information can be found in TDIF #306548 (DTN: SNF38040197001.001). Specifications for the gages are given in Appendix B of this report.

In addition to the 45 strain gages (15 rosettes) bonded to the CIP liner, there were five additional strain gages bonded to concrete and 304 stainless steel “coupons” placed near Canister #8 in the

Heated Drift. These “coupons” are prisms of concrete and steel that are used to provide baseline data on the strain gage response and some indication of unconstrained concrete material response. ESF-HD-RSG-16-EVL1 and ESF-HD-RSG-16-EVL2 were installed on sample prisms of the reinforced concrete used in the Heated Drift. ESF-HD-RSG-17-EVL1 and ESF-HD-RSG-18-EVL1 were installed on sample prisms of the nonreinforced CIP concrete used in the Heated Drift. ESF-HD-RSG-18-EVL2 was installed on a 304 stainless steel sample. The unconstrained CIP coupons are approximately 0.15 m × 0.15 m × 0.1 m and are instrumented with two strain gages attached in an orthogonal configuration on one of the flat surfaces, and the stainless steel coupon is instrumented with a single strain gage along the long axis of the coupon. The strain gages installed on the CIP coupons and the 304 stainless steel are identical to the gages attached to the inner surface of the CIP liner in the HD. The output from the CIP coupons provides an estimate of the unconstrained and therefore unstressed combined effects of concrete shrinkage and thermal expansion. The temperatures for each of these samples is estimated from thermocouples attached to the horizontal CDEX near the coupon locations (see Appendix C for thermocouple locations).

These strain gages have thermal expansion characteristics designed to provide a measure of mechanically induced strain on 304 stainless steel. In this case, the thermally corrected output from the strain gage is matched with the thermal expansion characteristics of the stainless steel, and should result in little or no change in strain as the unconstrained coupon is heated. However, to measure the total strain of the specimen, one must include the thermal expansion of the strain gage itself. The equation used to obtain the total strain measured by the strain gages is

$$\epsilon_{\text{actual}} = \epsilon_{\text{meas}} - \epsilon_T + \epsilon_{\text{sg}} + \epsilon_? \quad (4-2)$$

where

- $\epsilon_{\text{actual}}$  = actual, or total, measured strain deformation of the concrete
- $\epsilon_{\text{meas}}$  = strain calculated from the measured voltage for 1/4-bridge strain gage
- $\epsilon_T$  = temperature-induced apparent strain, corrected by manufacturer-supplied equation based on temperature
- $\epsilon_{\text{sg}}$  = strain correction calculated by  $\alpha_{\text{sg}} \times \Delta T$ , where  $\alpha_{\text{sg}}$  is the thermal expansion coefficient of the temperature compensated strain gage (for these gages,  $\alpha_{\text{sg}} = 8.5 \mu\text{strain}/^\circ\text{F} = 15.3 \mu\text{strain}/^\circ\text{C}$ , from BLH Electronics)
- $\epsilon_?$  = unknown strain correction due to other phenomena (difference between concrete and strain gage temperature-compensated for stainless steel, bonding effectiveness, etc.)

In the 1st Quarter data report, the total strains reported were calculated using the first two right-hand terms in Equation 4-2 (i.e.,  $\epsilon_{\text{actual}} = \epsilon_{\text{meas}} - \epsilon_T$ ). After discussions with strain gage experts from BLH Electronics and SNL, it was determined that this shortened equation is valid for measuring mechanical strain on a sample with the same thermal expansion characteristics as the strain gage, but is incorrect for determining the total strain on a heated sample with a different thermal expansion (e.g., concrete). To obtain the total strain (thermal + mechanical), the thermal expansion coefficient of the strain gage multiplied by the change in temperature should be included in the equation. The error term given in Equation 4-2 ( $\epsilon_?$ ) is included to indicate that such additional corrections were evaluated and, at this time, were found to have no or negligible

effect. Table C-4 in Appendix C of this report supersedes the same table in the April 1998 data report by presenting corrected strain data per Equation 4-2 at selected dates through the first and second quarters of the DST.

The data from the strain gages attached to the unconstrained CIP coupons are presented in Figure 4-39. The sign convention for the strain gages is positive for extension. The data from the unconstrained CIP samples show an initially large expansion during the first five days after heater activation. However, after 10 days, all four gages level off or decrease slightly at values ranging from 80-220  $\mu$ strain through day 72. Plots of displacement curves corresponding to constant thermal expansion coefficients of 8, 10, and 12  $\mu$ strain/ $^{\circ}$ C are also shown on Figure 4-39 for comparison. For a limestone-based concrete such as that used for the liner in the Heated Drift, a typical value for  $\alpha$  is 8  $\mu$ strain/ $^{\circ}$ C (Neville, 1997). Through 72 days, it is apparent that shrinkage due to dehydration of the concrete is affecting the strain deformation of the coupons. The contraction strain values indicated by Figure 4-39 are consistent with values reported by Neville (1997) for samples "dry" cured at 50% relative humidity. There does not appear to be any discernible difference in strain rate between the fiber reinforced and standard CIP thermal strains before 72 days. After 72 days, which is coincident with the local temperature reaching 96 $^{\circ}$ C (the local boiling point), strain rate changes representing expansion are measured for all four gages. This rate change would be consistent with the notion that the coupons are drying. Once the available water to the coupons has been driven away, a continued temperature increase yields an inflection in the strain measurements, resulting in a positive trend to the data. Two of the strain gages indicate an unconstrained expansion coefficient near 12  $\mu$ strain/ $^{\circ}$ C; the other two indicate higher values. It is unclear why the postboiling expansion coefficients are much higher than what would be expected for limestone concrete. There may be effects on the thermal expansion from other ingredients in the CIP coupons that have not yet been identified. The data from the concrete coupons will continue to be monitored.

The stainless steel strain gage response is presented in Figure 4-40. The strain gage bonded to the 304 stainless steel coupon exhibits nearly flat response to the change in temperature in the HD. As stated above, this response is expected, as the strain gages selected are compatible with stainless steel without temperature correction. This gage provides some assurance that the gages are expanding and performing as advertised.

The data presented in Figures 4-41 through 4-55 are for each of the fifteen strain gage rosettes bonded to the CIP liner inner surface. Figures 4-41, 4-46, and 4-51 show the strain gage data from the rosettes (RSG-1, RSG-6, and RSG-11) located at the crown of the Heated Drift at each of the three cross-sections previously described. Figures 4-42, 4-47, and 4-52 show strain gage data from the rosettes (RSG-2, RSG-7, and RSG-12) located on the right rib (south side) above the springline of the Heated Drift at each of the three cross-sections previously described. Figures 4-43, 4-48, and 4-53 show strain gage data from the rosettes (RSG-3, RSG-8, and RSG-13) located on the right rib (south side) near the invert of the Heated Drift at each of the three cross-sections previously described. Figures 4-44, 4-49, and 4-54 show strain gage data from the rosettes (RSG-4, RSG-9, and RSG-14) located on the left rib (north side) near the invert of the Heated Drift at each of the three cross-sections previously described. Figures 4-45, 4-50, and 4-55 show strain gage data from the rosettes (RSG-5, RSG-10, and RSG-15) located on the left rib (north side) above the springline of the Heated Drift at each of the three cross-sections previously described.

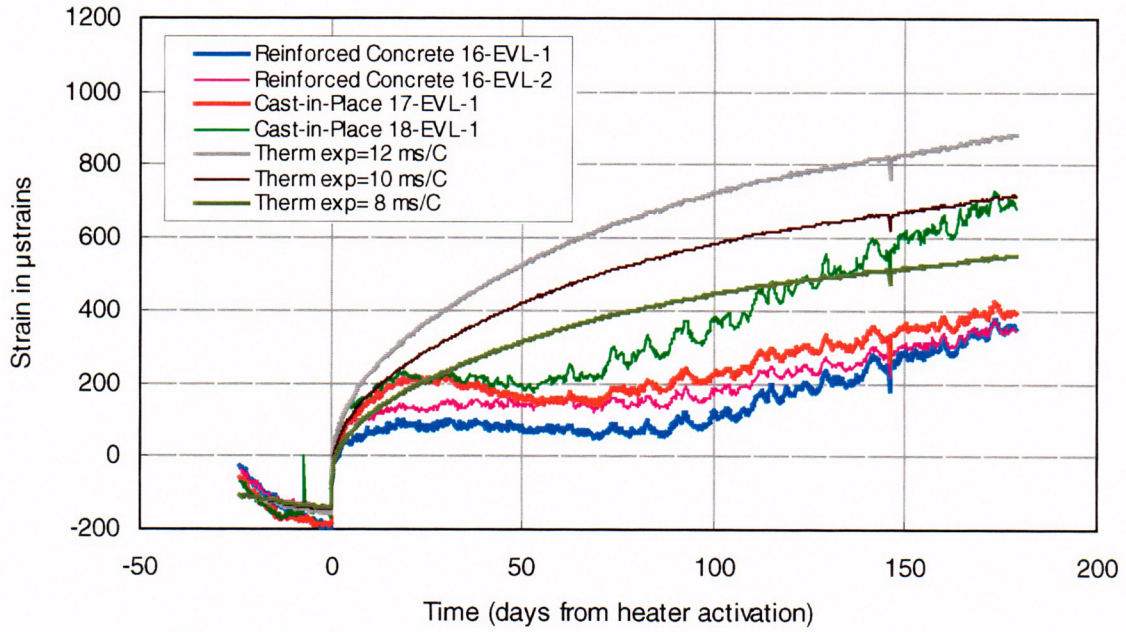


Figure 4-39. Measured strains for unconstrained CIP coupons.

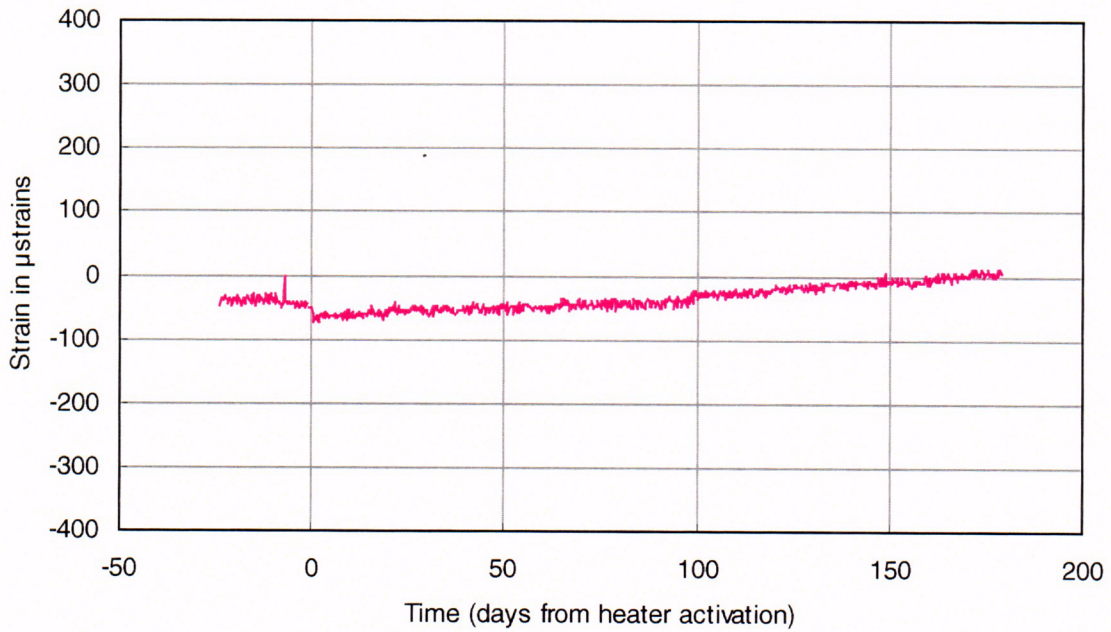


Figure 4-40. Measured strain for stainless steel coupon.

C43